OPTIMIZATION OF THE CONDITIONS IN THE MOLTEN SALT HYDRATE ASSISTED SYNTHESIS METHOD OF TIO_2

BY

CHENFENG HUANG

A thesis submitted to the

School of Graduate Studies

Rutgers, The State University of New Jersey

In partial fulfillment of the requirements

For the degree of

Master of Science

Graduate Program in chemical and biochemical engineering

Written under the direction of

Dr. George Tsilomelekis

And approved by

_____

_____

_____

New Brunswick, New Jersey

May, 2020

ABSTRACT OF THE THESIS

Optimization of the Conditions in the Molten Salt Hydrate Assisted Synthesis Method of TiO_2

by Chenfeng Huang

Dissertation Director: Dr. George Tsilomelekis

With the current transition in energy usage and concern for the environment, a primary goal is to find renewable and environmentally friendly catalysts with high activity and efficacy. To achieve this, advanced catalytic properties, such as high surface area, high acidity and low band gap energy, are of the utmost importance for heterogeneous catalysts. TiO_2 is one promising metal dioxides with good mechanical structure, prevalent in both Lewis and Bronsted acid sites, low band gap energy, non-toxicity and cost effectiveness. Synthesis of TiO_2 is itself not particularly novel. Sol-gel, hydrothermal, physical vapor deposition, and microwave methods have been widely studied for the production of titania. However, synthesis of TiO_2 via molten salt hydrates (MSHs) have limited exposure in the open literature. In MSH, ion-water interaction is optimized and water-water interactions are minimized; by changing ratios of water/salt and salt/precursor, modification of the structure, morphology and chemical properties of synthesized materials can be achieved. Therefore, the project was undertaken in order to understand how the MSH system affects crystalline growth and to synthesize TiO_2 with desirable catalytic properties.

In this work, Titanium Isopropoxide (TTIP) was utilized as the precursor, using a MSH-assisted sol-gel method to synthesize TiO_2 with varying properties by changing the ratio of water/LiBr and LiBr/TTIP. In order to understand the effect of the MSH system, XRD, N_2-BET, Raman, SEM, UV-vis and TPD-MS techniques were applied to characterize these samples. Likewise, TiO_2 phase transformation was observed to investigate thermal stability. Samples were calcined at different temperatures ranging from 400 to 600°C to observe phase transformation in TiO_2 using Raman; XRD was further used to quantify preponderance of anatase, brookite and rutile phases and to identify phase transition. Since TiO_2 serves as a semiconductor and photocatalyst, electronic spectroscopy was taken for all samples to measure the band gap energy via the Kubelka-Munk equation. To gain further insight into the potential of TiO2 as a material for acid-catalyzed reaction, identification and quantification of Lewis and Bronsted acid sites was conducted by pyridine and 2,6-dimethylpyridine TPD-MS.

The results show that all samples exhibit anatase and brookite phases. Utilizing Raman and XRD methods, it was found that brookite changes to anatase, which further transforms to rutile. Band gap energy of MSH TiO_2 was measured to be much lower than that of commercial anatase, brookite or even rutile. Moreover, a unique decreasing trend of band gap energy with increasing salt/TTIP ratio was observed. Based on results from TPD-MS, MSH TiO_2 is comprised of both Lewis and Bronsted acid sites, though these sites vary in quantity and strength. SEM images show MSH TiO_2 have flake-like morphology, and the thickness of these flakes decreases slightly with increasing ratios of salt/TTIP. BET surface area of some samples reaches to 200 m^2/g, which is much higher than that of commercial anatase. These promising properties highlight the potential of using MSH TiO_2 in future research and industrial applications, such as photocatalysis and alkylation reactions.

Acknowledgement

First of all, I need to appreciate my parents. Without their effort and sacrifice, I could not come to Rutgers University and study here. Secondly, I would like to express my heartfelt appreciation to Prof. Tsilomelekis, my knowledgeable advisor. Not only because of the knowledge he gave us in the Transport I class, but he also trained me to be a researcher. Through these two years of study with him, I got the basic knowledge of using some key technologies, like Raman.

Next, I want to thank my senior, Trang Tran. I followed her project, and she gave me lots of assistance in my work. Before I participated in this project, I followed with Thu Nguyen to do the DPR project; he is very knowledgeable and tried his best to help me in this work. Other than them, I would also like to thank Hedun Wang, Adam Zuber, Athanasios Kritikos, and Jakub Konkol; without their help, I could not finish my work.

Finally, I would like to appreciate Prof. Fuat Celik and other instructors from the Chemical Engineering Department. They gave me much assistance and lots of knowledge throughout the research process.

Contents

Figure list

Table list

1. Introduction

1.1 The development of heterogeneous catalysis and its industrial importance

Catalysis is among the most important concepts of modern chemistry and engineering. The wide range of catalytic applications in the chemical engineering industries have definitely change the way we live every day.[1-2] On one hand, the rational selection of catalysts from a technological point of view has the potential to improve the efficiency of many processes. On the other hand, concerning that the environmental pollution has become a serious problem in recent years, catalysis has played an essential role to mitigate or even provide multiple solutions to this problem. Therefore, studying catalytic applications with the perspective of understanding the synthesis and design of catalysts could help us a) understand the mechanism of chemical reactions but most importantly b) to control or even improve chemical reaction selectivity and overall efficiency.

Among the most important questions in the field of catalysis, those that are related to the design of catalysts and control of their molecular structure and properties are topical. Theoretical and experimental efforts on catalyst synthesis and design have advanced the field in the last century. These efforts have been placed towards designing catalytic systems that the prepared catalyst will lead to an increase of the reaction rate by decreasing its activation energy; of course, catalysts do not alter the thermodynamic equilibrium. Normally, catalysts are either solids or liquids. Based on the catalysts and the reactants phases difference, we could divide catalysts into two types: homogeneous and heterogeneous catalysts.[3]

The catalysts which has the same phase with reactants are called homogeneous catalysts. These are generally acid/base chemical compounds or some coordination complexes.[4] Generally, due to the higher homogeneity and dispersion of homogeneous catalytic sites in reactants, they show higher activity than heterogeneous catalysts. Since in an ideal scenario reactants and homogeneous catalysts are well mixed, the reactants molecules could react with the catalytic active sites much easier since no significant mass transfer/diffusion limitations are present. However, although high selectivity and overall activity can be achieved, the need of separation and reuse of active sites comprise the main disadvantages of homogeneous catalysis.

On the other hand, heterogeneous catalysis means that the reactions take place in several different phases. Usually, the heterogeneous catalysts are bulk solid materials and the reactants are gases or liquids.[5-6] The obvious advantage of utilizing heterogeneous catalysts, lies at the ease of separation from the reaction system; techniques like filtration or centrifugation for heterogeneous catalysts are much simpler than the distillation or liquid-liquid extraction for homogeneous catalysts underscoring their importance of use at the industrial level. Due to the

aforementioned reasons, heterogeneous catalysts have become a topic of great academic and industrial research with efforts to be placed on controlling the molecular structure, morphology and overall catalytic activity of various types of heterogeneous systems. [7]

Metal oxides comprise one among the most important and rather well-studied heterogeneous catalytic systems.[1-3] The diversified molecular structure of the active surfaces as well as their electronic and redox properties, metal oxides are very promising candidates for a wide range of chemical applications with immense impact to various industries. For example, atoms[8-9], clusters of atoms[10-12], hydroxyl groups[13] and other functional groups that can potentially be on the surface of metal oxides have the potential to result in well-controlled acid-based[14] and/or redox properties which in turn can favor their catalytic activity. Most commonly metal oxide like Al_2O_3, ZnO, SiO_2,[15-17, 20] and transition metal oxides like TiO_2, V_2O_5 and CrO_3 [18-20] have widely been used in industrial applications such as dehydrogenation, oxidation, alkylation etc[21-22]. In the present thesis the optimization of the synthesis conditions of a new synthesis method reported (*M*olten *S*alt *H*ydrate assisted) is studied, where TiO_2 nanosheets with high surface area can be tailored.

1.2 Crystal structure of TiO_2

Titanium dioxide is one of the most important and widely used transition metal oxides. The physicochemical properties of TiO_2 such as the high surface area, low band gap energy, thermal and chemical stability, non-toxicity etc. have made titanium dioxide to be widely used as photocatalysts, photovoltaic components, gas sensors in several industrial sectors including but not limited to manufacturing, aerospace, medical and biochemical engineering.[23] Its wide use as a catalyst support or even catalytic active site in a plethora of heterogeneous reactions is unquestionable and very rich literature can be found.[23-26]

Titanium dioxide (TiO_2) is a very important metal oxide which has been used in many fields. In nature, titanium oxide can be found in three different crystalline phases, i.e. Anatase, Rutile and Brookite. Fig. 1 shows the unit cell of these three different titanium oxides.

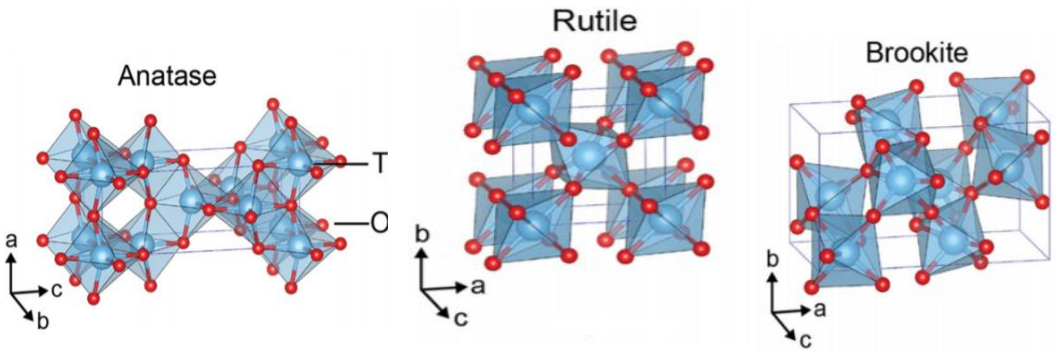

Figure 1 Three different phases of Titanium dioxide[26]

Anatase (a=b=3.785 Å, C=9.514 Å; space group D_{4h}^{19}, $I4_1/amd$) and Rutile (a=b=4.593 Å, C=2.959 Å; space group D_{4h}^{14}, $P4_2/mnm$), are represented both in a tetragonal crystal system; Brookite (a=5.143 Å, b=5.456 Å, C=9.182 Å; space group D_{2h}^{15}, *pbca*) belongs to an orthorhombic crystal representation.[23,27] In these three different crystalline structures, octahedral units of [TiO_6] are connected each other via corner-shared and/or edge-shared connections. In the anatase structure, each octahedron is surrounded by eight octahedrons including four corner-shared and four edge-shared, while in the rutile structure, each octahedron contacts with ten octahedrons included two edge-shared and eight corner-shared.[23, 27, 28] The three different crystalline phases could be altered under specific temperature and/or pressure conditions and thus understanding the effect of synthesis conditions on the crystalline structure is of great importance. According to thermodynamic data, the expected sequence for phase transformation follows the trend: anatase to brookite and finally to rutile[23, 27, 29]. Among the most used crystalline phases in catalysis, Anatase plays a crucial role because of its stability and high surface area. However, anatase to rutile transformation (ART)[23, 27, 29] is affected by many factors, like material properties, synthesis method and particle size and limits its potential for use in many high temperature chemical reactions.

1.3 TiO_2 serves as photocatalyst

As discussed in a previous section, research efforts in both academia and industry have been placed to replace traditional fossil fuel energy sources, by alternative energy resources. Towards this, photocatalysis plays an important role nowadays, since solar energy is an abundant and environmentally friendly alternative that has the potential to contribute the largest when compared to wind or tidal energy. The need of improving the properties of semiconductor materials has become a hot research topic in the photocatalysis field in an effort to improve process efficiency. A vast number of semiconductors have been studied such as TiO_2, ZnO, Fe_2O_3, CdS and ZnS[30].

TiO_2 serves as a potential semiconductor due to its low band gap energy (anatase: 3.2 eV, brookite: 3.02 eV, and rutile: 2.96 eV)[23,27], non-toxicity and low cost. Owing to its thermal stability, low band gap energy and advanced electronic surface structures, TiO_2 has become the most commonly applied semiconducting material. However, there are still some problems for photocatalysis with titania. The main challenge is that the undesired electron-hole back reaction occurs very easily, which results in less effective electron generation. Another challenge is the high band gap energy of TiO_2 compared to other semiconductors. As such, only ultraviolet light could excite electrons in TiO_2, but ultraviolet light only accounts for about 4% of solar radiation, while the energy from visible light accounts for approximately 50%[47]. To alleviate these problems, there are a number of methods. Loading pure metals on TiO_2 or adding the sacrificial reagents in the reactions to help reduce the undesired recombination reaction. Jerzy reported

Pt/TiO_2 catalysts that presented enhanced photocatalytic activity in water splitting by using different sacrificial agents.[30, 47-48] Wang improved the decarboxylation of fatty acids by inhibiting oligomerization, thereby alkane can be obtained in high yields, more than 90%.[31]

1.4 TiO_2 serves as catalyst support

Due to its nontoxicity, mechanical resistance and stability, TiO_2 can be utilized as a stable material in a wide range of conditions including acidic and oxidative environments. Anatase and rutile phases of titania are widely used in different reactions, such as dehydrogenation[40], water gas shift[41], thermal decomposition and hydrodesulphurization; brookite does not have such wide application.

Beside thermal stability, resistance to the corrosion and electrochemical stability, strong interactions between TiO_2 and supported materials make TiO_2 a promising catalyst support. There are mainly three types of support for TiO_2 based catalysts: TiO_2 as support in metal, metal oxide, bimetallic heterogeneous catalysts[7]. For example, metal/TiO_2 catalysts like Au/TiO_2, Pt/TiO_2 and Co/TiO_2 [30, 32-33]could be utilized in hydrodesulphurization of hydrocarbon oil and epoxidation of propane. CeO_2/TiO_2 and CeO_2/TiO_2 [39]modified by other metals like tungsten or metal oxides[49] like V_2O_5 have been synthesized to catalyze the reduction of NO_x by NH_3 because of significant Bronsted acidity and electronic interaction between different metal oxides and TiO_2, resulting in high selectivity[39]. $AuCu/TiO_2$[40] is employed in oxidation of methane, ethane and propane, and $CuZn/TiO_2$ is used to catalyze C_2-C_4 olefin have been reported.[41] Therefore, TiO_2 is a promising catalyst support and can be further developed for other applications.

1.5 Common synthesis methods of TiO_2 materials

The wide range of applications for TiO_2 due to their different physicochemical properties has sparked research interests from the materials synthesis and design perspective. Understanding the proper way to modify the molecular structure, crystallinity and morphology of catalytic materials, requires intense efforts towards unravelling the phenomena occurring during the synthesis steps. Towards this direction, intense research efforts by many people have led to the development of a large number of different synthesis protocols and techniques which in turn result to the synthesis of metal oxide materials with controlled properties. Next, we discuss some typical synthesis methods that pertain to TiO_2 (but also to other metal oxides). In addition, we discuss some common characterization techniques that routinely utilized and are in-line with the work that has been done in the present thesis.

1.5.1 The sol-gel method

The sol-gel method[23, 34-37, 63] is a very common method to synthesize metal oxide materials. In general, there are two crucial steps in the sol-gel method, i.e. the hydrolysis and the

condensation step. In the sol-gel process, a colloid is formed in the first hydrolysis step; in the condensation step, the polymerization reaction shown in Fig 2 will occur, resulting in a metal hydroxide network. Finally, it is necessary to remove any remaining salts and alcohol unreacted species. Titanium (IV) alkoxides[37] are typical precursors applied in TiO_2 synthesis. Titanium Isopropoxide (TTIP) and titanium ethoxide are examples that have been widely studied.[34-37]

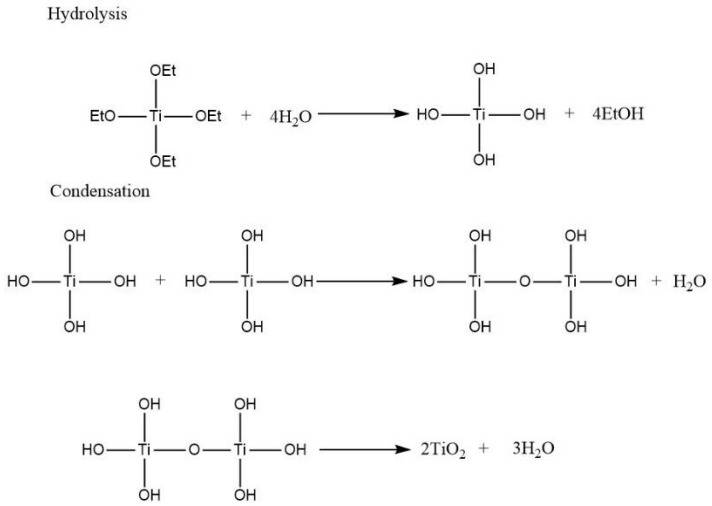

Figure 2 Sol-gel process of Titanium ethoxide[37]

There are, however, some practical considerations that have to be taken into account during titania synthesis. Hydrolysis happens immediately when the alkoxide precursor comes in contact with water. Therefore, in the sol-gel method, the concentration of water plays a very important role that controls many properties such surface area, particle and agglomerate size, crystal structure and crystallinity etc. In principle, high concentration of water will increase the hydrolysis ratio to form $Ti(OH)_4$; however, large quantities of water will reduce the rate of the condensation process, which is necessary to form the well-ordered three-dimensional polymeric structure of TiO_2. Insufficient condensation of $Ti(OH)_4$ units could hamper the formation of polymeric chains of Ti-O-Ti structure, resulting in loosely-packed titanium oxide particles. The kinetics of the condensation reaction have been rationalized in the Lifshita-Sliovoz-Wagner (LSW) model.[38] A time and temperature dependent study by Gerko shows that the rate of coarsening in the condensation could affect also particle size[38]. Consequently, although the relatively simple sequence of steps in sol-gel synthesis, parameters like water, reaction time and synthesis temperature are essential towards controlling the properties of TiO_2.

1.5.2 The hydrothermal method

The hydrothermal method, also referred to as hydrothermal/solvothermal method, is another basic and commonly applied method. Typically, a precursor solution is placed in a closed steel vessel capable of maintaining high temperature and pressure. In the hydrothermal system, particle growth and assembly occur in the reaction medium, which is normally water. Reaction

medium properties could highly affect the final structure and morphological characteristics of the synthesized materials. The advantage of the hydrothermal method is related to the particle growth and nucleation in homogeneous solutions. In this way, the nucleation rate could be controlled via manipulation of different conditions of the solution system such as pressure, temperature, pH, time etc. Lee[35] reported the hydrothermal synthesis of titania from titanium butoxide ($Ti(OBu)_4$) precursor under acidic conditions. The following reaction represents the overall hydrolysis and condensation steps for this case.

$$Ti(OC_4H_9)_4 + (2+x)H_2O \rightarrow TiO_2 \cdot xHO_2 + 4C_4H_9OH$$

As a result, in this work the authors were able to form titanium oxide mixtures of anatase and rutile. These mixtures showed high stability, with a transformation temperature of approximately 1100 °C, which is much higher than the normal anatase-rutile transition temperature.

1.5.3 The molten salt hydrate (MSH) mediated synthesis

Salt-water systems are defined by the proportion of salt to solvent, ranging from infinite dilution to state of molten salts. These systems are demonstrated in Fig 3, illustrating the interaction between water molecules and salt cations. Molten salt hydrates is a specific designation given to intermediate salt-water systems that lie in between the extreme of infinite dilution and molten salts.[43-46] In an ideal MSH, the cation of salt is surrounded by water molecules in a single hydration sphere, while the anions are free in the solution. Some cations like Li^+, Mg^{2+}, Ca^{2+} or Zn^{2+} exhibit this behavior when the ratio of water/salt is in a specific range[44]. Normally, MSH has one basic principle, i.e. that the molar ratio of water/salt should be below or equal to the coordination number of the cation. For Li^+, the coordination number based on computational calculation is 3-6, and the accepted ratio of water to salt is 3-4:1[43].

MSH at a specific water-salt condition have been used as a solution medium for cellulose hydrolysis in the presence of small amounts of acids. For example, $ZnCl_2$, $CaCl_2$ and LiCl could solubilize cellulose[45]. Due to the presence of solvent molecules, the salt is able to form coordination bonds with cellulose and negate hydrogen bonding. Furthermore, by performing the reaction with MSH in the presence of a non-derivatizing solvent,[59] cellulose to glucose conversion could be improved up to 98%[44]. Likewise, due to the ion-water interactions specific to MSH, it displays significant properties, such as low water activity, enhanced viscosity and tendency of supercooling[55]. Therefore, in MSH medium, material properties and morphology have the potential to improve and augment. In this thesis, we apply the MSH technique reported [55]elsewhere to synthesize titanium oxide, while varying the water/salt ratio to observe its effect on morphology and material properties.

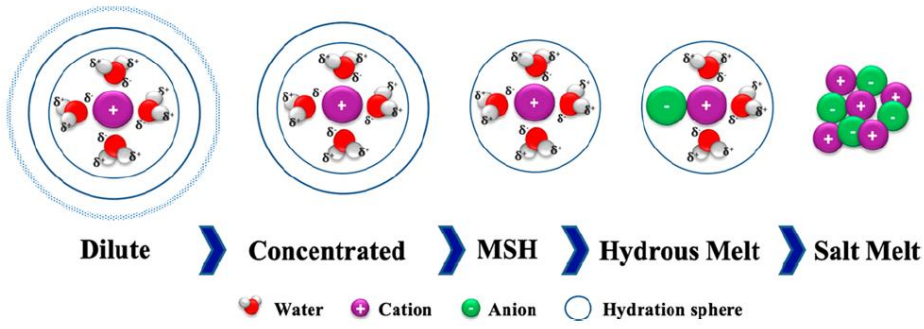

Figure 3 Interaction between water and cation[43].

1.6 Scope of this work

Titanium dioxide has a wide range of applications in many fields due to its favorable physical and chemical properties. The open literature has been preoccupied with attempts to optimize TiO_2 synthesis to augment and enhance these properties. One potential way to do so is via molten salt hydrates (MSH). Using this method is nontrivial and is a rather daunting task, highlighting the importance of this work. The main parameters that are prioritized in this work are:

- Water/LiBr ratio
- LiBr/TTIP ratio
- Calcination temperature
- Effect of H_2SO_4 and NH_4 ions during the synthesis

Characterization of titania materials synthesized via MSH was achieved using:

- XRD
- Raman
- UV-vis,
- SEM
- Pyridine/2,6-dimethylpyridine TPD-MS
- N_2-absorption.

These variegated techniques allow for understanding the structure, morphology, electronic structure, abundance and nature of acid sites, and surface area, to name a few. Likewise, it is possible to identify the transition between the three phases of titania at different calcination temperatures. Overall, this work strives to determine the effect of the MSH condition on these materials.

2. Experimental techniques and relevant considerations

2.1 Raman spectroscopy

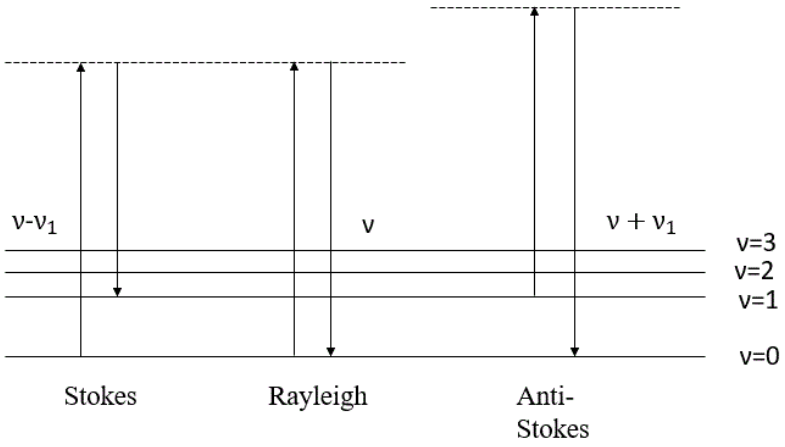

Figure 4 Raman scattering and Rayleigh scattering

Figure 4 shows the elastic and inelastic scattering process that occurs when matter interacts with light. The term Raman phenomenon was introduced in 1922 by the Indian physicist C.V. Raman where he firsts discovered this process.[50-53] Raman spectroscopy has become one of the most common spectroscopic techniques to characterize the structure, active sites and surface species on metal oxide materials. Nowadays, considering the further development and advances of this technique, Raman spectroscopy holds a very important role for modern researchers to understand catalysts under real reaction condition (Operando Raman spectroscopy), interaction of various species in synthesis, medical science and pharmaceutical development, nanomaterials etc.

Raman spectroscopy is an inelastic scattering of light process. When UV, visible light or near infrared light interacts with a substance, absorption and/or scattering of the incident light occurs. The incident beam promotes the excitation of a molecule to a virtual state (a short-lived state) after which the molecule returns to the ground state. This scattering process can be described via three different processes:

- **Rayleigh scattering**: Excited molecules reemit photons in all directions without changing frequency level. In this process the light is elastically scattered i.e scattered light has the same energy as the incident light
- **Stokes scattering:** A small number of photons, (~1 photon in 10^6) will scatter at a higher frequency than the incident photons thus giving scattered light at frequency of ν-ν_1.

- **Anti-Stokes scattering:** When the scattered light loses energy during this process (initially at an excited state) then the system reaches a lower energy level thereby giving scattered light at frequency of $\nu+\nu_1$.

2.2 X-ray diffraction spectroscopy

X-ray was discovered by W.C. Rontgen in 1895. After having been developed by W.L Bragg and W. Friedrich, in 1921, P.P. Ewald refined the basic theory of X-ray diffraction (XRD). Since then, XRD has become an intriguing technology to understand the phase structure, crystallite size and strain in nanomaterials.

In modern solid-state chemistry, a crystal could be considered a set of discrete parallel planes separated by distance *d*. Here, we consider these parallel layers as diffraction grating. When the crystal material is exposed to X-ray radiation, reflectance occurs on the atoms of these planes separately. Constructive interference occurs when the length of two waves is equal to an integer multiple wavelength. This can be expressed by Bragg's Law as follows[50-53]:

$$n\lambda = 2dsin\theta$$

where *n* is the diffraction order, λ is the wavelength, and *d* is the interatomic distance. Fig 5 is a physical depiction of Bragg's Law.

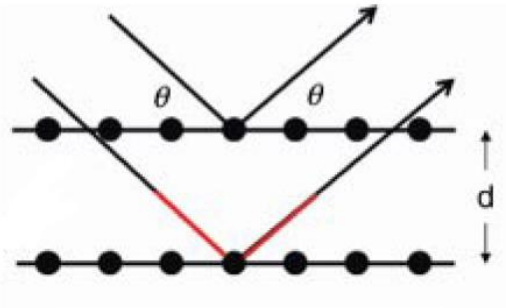

Figure 5 Bragg law[50]

Bragg peaks are affected by the crystallite size. Particle size is calculated based on the Scherrer equation[50]:

$$D = \frac{k\lambda * 57.3}{\beta \cos\theta}$$

where D is the crystallite size, λ is the wavelength, β is the peak width in degree 2θ, and *k* is a constant.

Since X-ray diffraction offers many advantages, this technology has been widely used in the characterization of crystalline materials, including phase identification and quantification, crystalline domain size and shape, lattice strain and strain effect, and catalysts in a reactive atmosphere. TiO_2 is a material that can effectively be characterized via XRD to identify properties of significance. For example, it is of prime importance to identify and distinguish

between the three phases of titania, i.e. anatase, rutile, and brookite; likewise, it is also necessary to understand the degree of crystallinity; these properties are readily analyzed using XRD.

2.3 SEM of TiO_2

Scanning electron microscopy (SEM) is an integral method to see the surface properties and morphology of nanomaterials. Human eyes could distinguish 0.2 nm apart if the light source is sufficient. Modern light microscopy could improve the magnification by about 1000 times. However, the average wavelength of white light is about 550nm, resulting in poor resolution. Scanning electron microscopy emits a high energy beam of electrons on the material's surface; since the electrons have very short wavelength, this technique improves image resolution significantly.

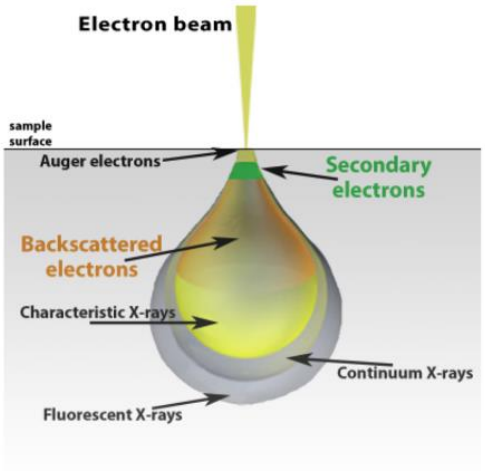

Figure 6 Schematic of electron beam interaction[52]

Under vacuum conditions, a high energy electron beam is emitted by an electron gun and passes several condenser lenses to focus on the surface of the sample. Secondary electrons, backscattered electrons and characteristic X-ray are produced several microns below the surface. These three signals go through specific directors and produce the image on a computer. Normally, SEMs could provide resolution between 1-20 nm; some could provide even below 1 nm, based on the electron spots size and material.

2.4 Surface area and porosity measurements

For heterogeneous catalysts, surface area, porosity, pore volume, and structure are intrinsic properties of porous materials. Gas adsorption technology has been evolved and applied in characterization of surface area and porous structures of various materials. Several theories have been developed. The Langmuir model is a basic theory of the adsorption process. There are four principles: (1) there are some adsorbing sites on the surface of the adsorbent, and the adsorbate could only bind on these sites to form a single layer; (2) the adsorption energy for all sites are equal; (3) there are no interactions between adsorbent molecules, and interactions only appear between adsorbate molecules and binding sites; (4) adsorption and desorption reach equilibrium. The Langmuir adsorption model is expressed by the following equation[50-53]:

$$\theta = \frac{V}{V_m} = \frac{\alpha p}{1 + \alpha p}$$

where θ is the fractional occupancy of adsorption sites, V_m is the volume of the monolayer, V

is volume of the adsorbate onto solid absorbent, α is the equilibrium constant, and p is the partial pressure. However, the Langmuir model describes an ideal adsorption, in that it assumes that only monolayer adsorption occurs and that there is no interaction between adsorbent molecules. To improve this model, S. Brunauer, P.H Emmett and E. Teller (BET) modified the Langmuir model to a more realistic and well-established adsorption theory (BET). In BET adsorption theory, they complemented three assumptions; (1) adsorption is not monolayer; (2) the enthalpy of adsorption (E_1) for the first layer is the molecular interaction with solid material; and (3) the enthalpy of adsorption (E_L) between the first layer molecular and second layer (or higher) is the same as the enthalpy of liquefaction. Based on these assumptions, they modified the Langmuir equation to infinitely adsorption BET equation:

$$\theta = \frac{V}{V_m} = \frac{Cp}{(p_0 - p)[1 + (C-1)\frac{p}{p_0}]}$$

where $C = C_0 \exp\left(\frac{E_1 - E_L}{RT}\right)$

V_m is the volume of the monolayer, V is volume of the adsorbate on a solid adsorbent, p is the equilibrium pressure, p_0 is the saturation pressure, C is a constant which relates enthalpy of E_1 and E_L. The BET equation is one of the most famous models to characterize heterogeneous catalysts and has been widely used from the time it was published until modern times. Titania is a porous material whose pore volume, pore diameter, and surface area can be facilely classified via BET.

2.5 UV-vis

Electronic spectroscopy, also known as UV-vis spectroscopy, is a technique to identify the electronic structure of materials. This technology could be used not only for liquid but also solid materials. Meanwhile, because of its high sensitivity and fast collection, UV-vis plays a very important role in the surface characterization of modern heterogeneous and homogeneous catalysts as well as in reaction kinetics studies.

The principle basis of electronic spectroscopy is electronic transition theory. Based on modern chemical orbital theory, electronic energy levels are discrete and follow the order of E_0, E_1, $E_2 \ldots E_n$ according to the Schrodinger equation. The electrons on E_n could absorb energy from photons and transit to the E_{n+1} energy level. This energy change is based on the valence electrons and has no bearing on the inner shell electrons. The aforementioned electronic transitions reflect on the properties of materials, such as band gap, thus highlighting the significance of UV-vis spectroscopy.

As discussed before, UV-vis spectroscopy could be utilized in liquid phase and solid phase.

There are unique theories to describe electronic transition in each phase. For the liquid phase, the Beer-Lambert law has been used as follows[50-53]:

$$A = log_{10}^{(\frac{I}{I_0})} = \varepsilon cL$$

A is measured absorbance, I_0 is the intensity of the incident light, I is the transmitted light intensity, c is the concentration, L is the path length of the light, and ε is the molar extinction coefficient. Based on this equation, after measuring the intensity of transmitted light through a liquid material, it becomes possible to quantify the concentration in the liquid phase.

The second method to describe solids and powder materials is reflection and diffuse reflectance spectra. By this method, reflection and diffuse reflectance occurs when the sample is under UV radiation. Here the term "reflectance" refers to the light intensity difference between the incident light and the reflectance. Thus, the reflectance could be given by $R=I/I_0$ ($0<R<1$). The reflectance case is not proportional to the concentration compared to transmission. Reflectance could be controlled by various parameters, like particle size, absorption coefficient wavelength and the regular reflection. UV-vis spectroscopy is an effective technique to quantify band gap energies in heterogeneous catalysts, thus underlying the importance of implementing this method to characterize TiO_2.

3. Experimental

3.1 Materials

Titanium (IV) Isopropoxide, (99.99% trace metals ba-sis), lithium bromide (ReagentPlus®, ≥99%) and titanium (IV) oxide (Brookite and Rutile), Pyridine, (, 99.8%) and 2,6-dymethylpyridine, (, ≥99%) were purchased from Sigma–Aldrich and used without further purification. Titanium (IV) oxide (Anatase, Rutile and Brookite) for reference were purchased from Alfa Aesar.

3.2 Catalyst synthesis

Herein, we describe the sequence of the synthesis steps. There are three mainly processes: preparation of the molten salt hydrate solution, precipitation and calcination. Firstly, we dissolve appropriate amount of LiBr in 15ml deionized water. In order to follow the MSH state, we change the water/salt ratio only within the 3.25, 3.75, 4 and 4.5 regimes. The solution s stabilized in an oil bath at 35 ℃, under stirring for about 30mins. After the temperature is stable and make sure that all LiBr is fully dissolved in water, we add pre-calculated amount of titanium isopropoxide (titanium precursor) in the solution. Here, we control the salt/TTIP molar ratio change from 13, 50, 80 and 120 while keeping the water/salt ratio constant. After adding TTIP, we observe the formation of gel-like particles immediately. We maintain the temperature and stirring speed constant for 1h in order to ensure complete hydrolysis and significant extent of condensation in the solution. Next, we wash thoroughly the samples by using 500ml deionized water via a Büchner funnel to filter the samples under vacuum conditions. Drying of the samples was followed in an oven at 110 ℃ for overnight. The dried samples were next calcined at 400 ℃ for 3h with a ramping of 2℃/mins in air flow of 100 cc/min. To investigate the effect of temperature of calcination, a 3.25-13 sample is divided in 5 parts, where each part was calcined at 400, 450, 500, 550 and 600 ℃ under the same condition. Further characterization of all these samples were performed as described next.

Figure 7 Synthesis materials

pH is a very important parameter for synthesis system, especially for sol-gel method, since it might change the condensation process in sol-gel system. In an effort to investigate the effect of the presence of basic conditions, 2 ml of ammonium hydroxide was added in solution. Using pH probe to measure the solution pH and then synthesis 3.25-13 (water/salt-salt/TTIP) sample.

Calcinating this sample at 400, 450, 600, 700 and 800 ℃.

3.3 Catalyst Characterization

3.3.1 X-ray diffraction

XRD spectra were collected by Philips XPert system with seal-tube Cu anode, mini proportional counter detector, graphite monochromator, programmable receiving slit, sample charger and sample spinner.

Table 1 Parameters of XRD

Parameters	Values
Scan type	Gonio
2 theta range	20-80
Stepsize	-0.02
Time (s)	0.5
Spinner	8 sec/revolution
Generator voltage (kV)	45
Tube current (mA)	40

3.3.2 Raman spectroscopy

Raman spectra were recorded using a Horiba LabRAM HR Evolution high spatial and spectral resolution spec-trometer. The incident beam (532nm, 80mW) was di-rected into a reaction cell (Harrick Scientific Products Inc.) and focused on the sample with a 10x long-working distance objective. Collection of the scattered light was achieved with an air-cooled (-75°C) open electrode 1024x256 pixels CCD. The acquisition time of each spectrum was 20-60secs, the number of accumulations varied in the range of 6-12 and the spectral slit was fixed at 100µm. A 25-50% neutral density filter was also used to avoid local overheating of the catalyst sample which can cause changes in the measured spectra. For the in-situ Raman calcination measurements, air flow is maintained at 50-100cc/min via a mass flow controller (Alicat Scientific). All spectra were produced in dark condition to hamper white light interference in the spectral background. To get the perfect resolution and more information, 10x and 100x objective were used for all samples and relevant parameters are listed in Table 2.

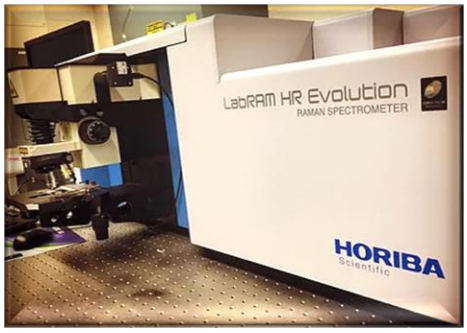

Figure 8 Raman spectroscopy

Table 2 Parameters of Raman spectroscopy

Parameters	Values
Acquisition time (s)	5-10
Accumulation	3-15
Objective	10x or 100x
Grating	1800 gr/mm
ND Filter	25%
Laser	532 nm

3.3.3 UV-vis spectroscopy

Samples were loaded into a micro sample cup loosely filling volume to be 0.022 ml. UV-visible spectra were collected inside a Harrick Scientific Praying Mantis diffuse reflectance accessory with Xe beam and detector from Thermo Scientific Evolution 3000 spectrophotometer. The range of wavelength scanning was between 190 nm to 1100 nm with intervals of 2.0 nm. Absolute reflectance standard was collected using a Spectralon® disk.

Figure 9 UV-vis

3.3.4 SEM and Nitrogen absorption

Scanning electron microscopy (SEM) images were acquired with a Zeiss, Zeiss Sigma Field Emission SEM. Transmission electron microscopy (TEM) images were acquired with a JEM-2010F (JEOL, Japan) transmission electron microscope equipped with a field emission gun (FEG) emitter. The specific surface area of the prepared TiO2 samples was estimated through Brunauer-Emmett-Teller method (BET) using a Quantachrome, Autosorb-1 instrument. The BET measurements were carried out at liquid nitrogen temperature after degassing samples at 150°C for 3 hours.

3.3.5 Pyridine and 2,6-dimethylpyridine TPD-MS

To identify and quantify the Lewis acid sites and Bronsted acid sites, pyridine and 2,6-dimethylpyridine TPD has been conducted for water/salt ratio from 3.25-4.5 with salt/TTIP ratio is 13 by using mass spectrum (MKS, CIRRUS 3-XD). First, the MS was calibrated to a set flow of pyridine or 2,6-dimethylpyridine in nitrogen. To conduct TPD, adsorbate (pyridine or 2,6-dimethylpyridine) was loaded into a bubbler. A gentle flow of nitrogen gas (30 sccm) was introduced to the bubbler and sent to a Harrick cell, in which the sample was loaded. Carrier gas flow rate was fixed to make sure the total pressure is constant. Once the species was fully

adsorbed on the sample, nitrogen flow was cut off from the bubbler and sent directly to the Harrick cell, so as to remove any physisorbed species. When detection of adsorbate was minimized, a temperature program was started, such that sample temperature was increased at a rate of 5°C/min; evolution of adsorbate was monitored via MS.

To calibrate the MS and quantify the amount of adsorbate, Raoult's law could be used, given the high purity of pyridine and 2,6-dimethylpyridine. Bubbler calibration is calculated based on the flowing equation.

$$\mathrm{F_{V,out}} = \mathrm{F_{c,in}} \frac{\mathrm{P_V}}{\mathrm{P_{head}} - \mathrm{P_V}}$$

$\mathrm{F_{V,out}}$ is the vaper flow of the pyridine, $\mathrm{F_{c,in}}$ is the carrier gas flow rate, $\mathrm{P_V}$ is the vapor pressure of the pyridine, $\mathrm{P_{head}}$ is the atmosphere pressure.

To calculate $\mathrm{P_V}$, the Antoine equation can be invoked.

$$\log_{10} \mathrm{p} = \mathrm{A} - \frac{\mathrm{B}}{\mathrm{C} + \mathrm{T}}$$

The specific Antoine constants for pyridine at 25℃ can be obtained from the NIST database, as follows:

A = 4.16272; B = 1371.358; C = -58.496;

Applying the Antoine equation above, the vapor pressure of pyridine is 0.027 bar. Based on the bubbler calibration equation above, the flow of pyridine is $F_{v,out}$ = 0.83 sccm. Given that the total flow is approximately 30 sccm, the percentage of pyridine flow in the gaseous stream is about 2.8%. This value was used to calibrate the MS.

After performing TPD, the Cirrus 3XD software provided the concentration of pyridine evolved during desorption. This quantity was converted to volumetric flow of pyridine using the following equation:

$$\frac{(\%\ concentration\ pyridine)(30\ sccm\ total\ volumetric\ flow)}{1000\ mL/L} = volumetric\ flow\ of\ pyridine\ (L/min)$$

The molar flow of pyridine was then estimated using the ideal gas law:

$$\dot{n} = \frac{P\dot{V}}{RT} = \frac{(1\ atm)\dot{V}}{(0.08206\ L \cdot atm/mol \cdot K)(298\ K)}$$

By integrating the molar flow of pyridine over time, it is possible to determine the total amount of pyridine desorbed from the sample. If it is assumed that one molecule of pyridine adsorbs onto each acidic site, then the total number of acid sites can be determined.

4. Results

4.1 The Raman spectra of synthesized TiO_2 samples

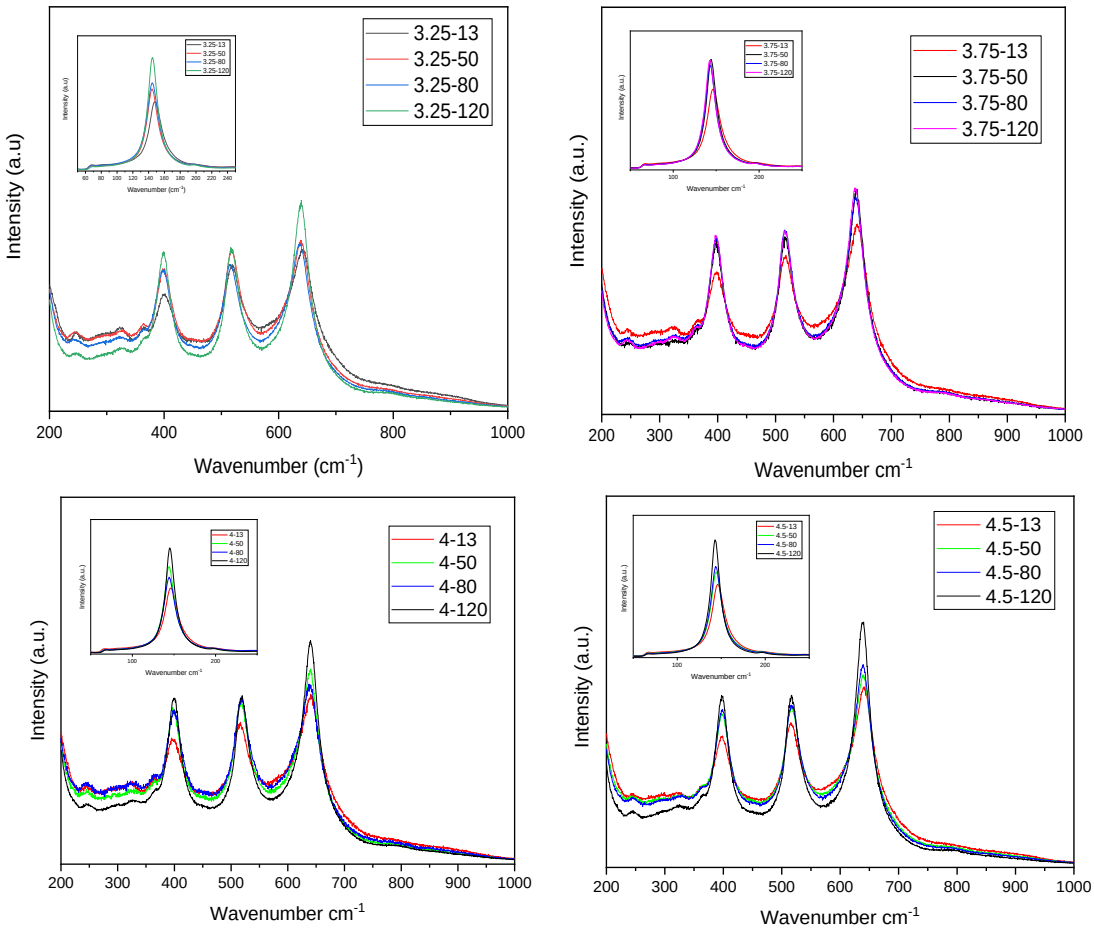

Figure 10 Raman shift of different water/salt and salt/TTIP ratios

Raman spectra for all water/salt ratio 3.25-4.5 and salt/TTIP ratio from 13-120 at 400 °C calcinated samples have been showed in Fig 10. According to the factor group analysis, anatase has six Raman modes ($A_{1g}+2B_{1g}+3E_g$) and these Raman bands are identified at 144 cm^{-1}, (E_g, ν_6), 197 cm^{-1}, (E_g, ν_5), 399 cm^{-1}, (E_g, ν_4), 513 cm^{-1}, (E_g, ν_3), 519 cm^{-1}, (B_{1g}, ν_2) and 639 cm^{-1}, (E_g, ν_1) respectively at room temperature[45]. The nature Brookite has 69 optical modes ($9A_{1g}+9B_{1g}+9B_{2g}+9B_{3g}+9A_{1u}+8B_{1u}+8B_{2u}+8B_{3u}$) depending on the factor group analysis. These modes A_{1g} (127, 154, 194, 247, 412, 640 cm^{-1}), B_{1g} (133, 159, 215, 320, 415, 502 cm^{-1}), B_{2g} (366, 395, 463, 584 cm^{-1}), B_{3g}(452 cm^{-1}) are well identified[46]. From Fig 12, four high intensity peaks of anatase crystalline form at about 147 cm^{-1}, 399 cm^{-1}, 519 cm^{-1} and 639 cm^{-1} are clearly observed. A closer look in the spectral regime of 200 to 350 cm^{-1}, some low intensity peaks could be observed, which are assigned to the presence of brookite phase. The result shown in Figure 12 of all samples tested herein demonstrate the presence of TiO_2 with both anatase and

brookite; however, we have to notice that anatase is the main crystalline phase.

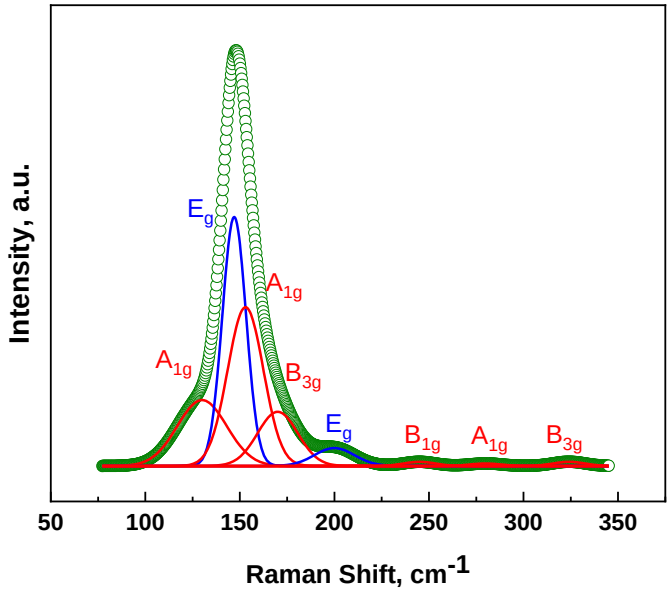

Figure 11 Deconvolution peaks of anatase and brookite[47]

It is worth to mention that when the salt/TTIP ratio change from 13 to 120 at a specific water/salt ratio, a clear increase in the intensity of anatase peaks is observed. This observation demonstrates that the fraction of crystalline anatase increases as the salt/TTIP ratio increases. Focusing on our Raman spectra carefully, a slight Raman shift from 147 to 144 cm^{-1} and 640 to 638 cm^{-1} occur when the water/salt is 3.25 and salt/TTIP ratio is 13 and 120. Trang et. Al[47]. showed via spectral deconvolution (Fig11) that the main anatase vibrational peak at about 147 cm^{-1} has a clear contribution from both the Eg (ν_6) of anatase as well as the A_{1g} and B_{3g} vibrational modes of brookite. These vibrational modes overlap mutually and result in this 147 cm^{-1} slightly asymmetric character. On the other hand, a slight Raman peak shift from 147 to 144 cm^{-1} when the salt/TTIP ratio increase from 13 to 120 at the water/salt ratio equal to 3.25 reveals qualitatively that the amount of brookite in this systemic trend is decreasing. Combining with the decreasing intensity of brookite Raman vibrational bands in the range 200-350 cm^{-1}, it is safe to suggest that the anatase Eg (ν_6) vibrational band increases and brookite A_{1g} band decreases, which result in a 3 cm^{-1} Raman shift. Similar behavior, which could be represented by the relative intensity change between anatase and brookite peaks (Fig 12), was also observed in the case of synthesis of TiO_2 at different water/salt ratio such as 3.75 to 4.5 and relevant results are summarized in Figure 13. The increasing amount of anatase phase might be associated with the amount of water present in MSH, which result in increasing hydrolysis and

condensation rate. The results presented in this section highlight the possibility of controlling the relative amount of the different TiO_2 crystalline phase during the synthesis process; i.e by controlling water/salt and salt/TTIP ratios, the anatase/brookite ratio can be controlled.

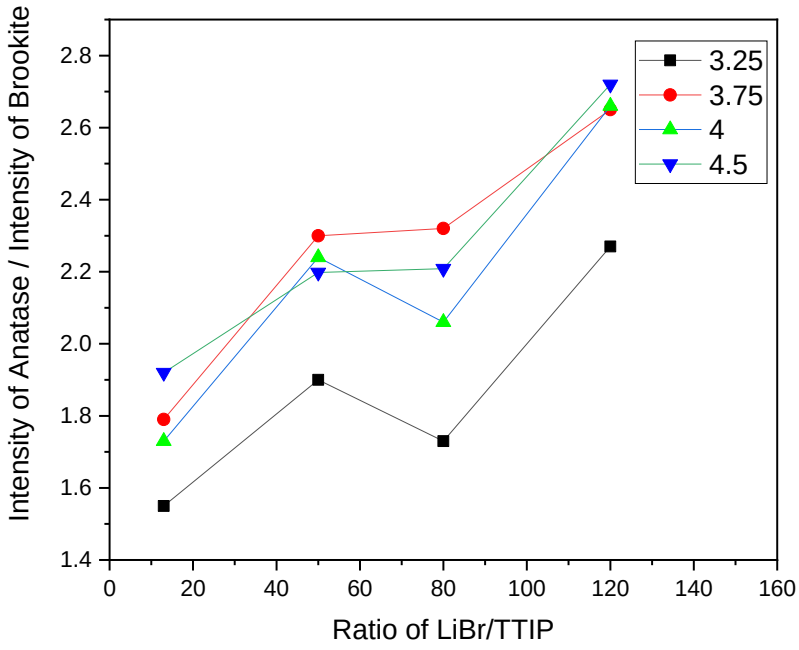

Figure 12 Intensity of anatase/brookite ratio for different samples.

4.2 Effect of water/LiBr ratio on the Raman spectra of synthesized TiO_2 samples

We vary the ratio of water/LiBr in the synthesis of TiO_2 in an effort to investigate possible changes in the crystal phases, morphology as well as physicochemical properties. Fig 13 shows the Raman data of samples, which water/salt ratio ranges from 3.25-4.5 at fixed salt/TTIP ratio at 13. As can be seen, the anatase bands are the dominant ones while low intensity brookite bands are always present in the frequency regime of 200-350cm^{-1}. This result suggests that almost independently on the salt/TTIP ratio, brookite has the tendency to be formed in highly concentrated MSH solution media. However, we have to mention here that upon increasing the water/salt ratio, the amount of brookite decreases while at the same time a slight increase in anatase's crystallinity can be observed (sharpening of 145cm^{-1} band).

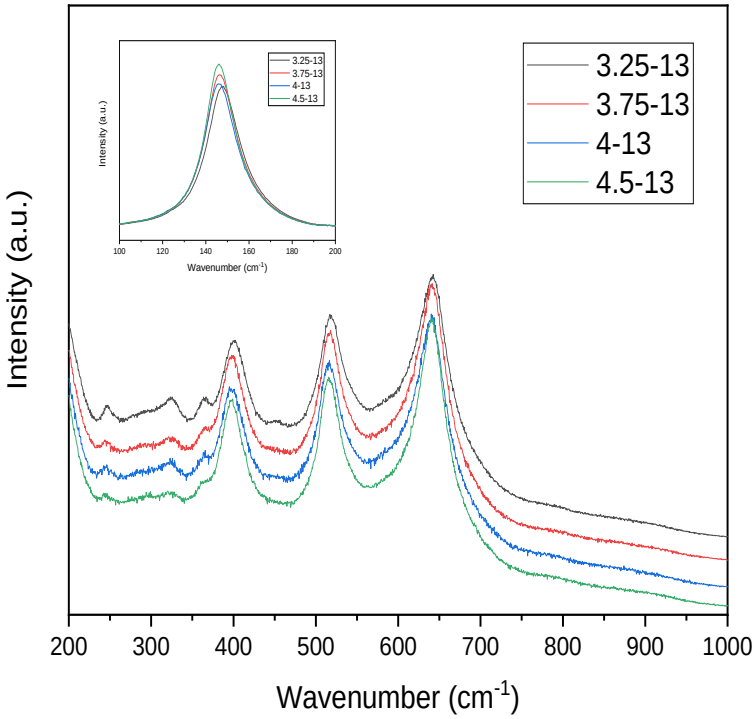

Figure 13 Raman spectrum of different ratio of Water/LiBr

Based on Fig 13, it is easy to observe the intensity of anatase main peaks at about 147 cm^{-1}, 399 cm^{-1}, 519 cm^{-1} and 639 cm^{-1} have an increasing trend obviously with brookite bands decreasing. Meanwhile, a small shift of 147 cm^{-1} to 146 cm^{-1} could be observed when the water/salt ratio change from 3.25 to 4.5. Combining with the previous deconvolution result by Trang[47], it is apparently that the water/salt ratio is an essential parameter. In the meantime, the XRD data can be used to quantify the amount of anatase and brookite different phases in these materials.

XRD diffractograms have been taken for four samples with salt/TTIP ratio 13 and varying water/salt. Two clearly phases can be seen in Fig 14. The strong diffraction peak at 25.4º (2θ) is characteristic for the anatase [101] while the small peak located at 30.81º (2θ) is ascribed to the brookite [121]. By analyzing the XRD results of Fig.14, a decreasing trend of the amount of brookite with increasing the ratio of water/LiBr is observed, result that is in great agreement with our Raman spectral analysis discussed above. Table 3 summarized the amount of brookite and anatase phases in these materials respectively. When the water/salt ratio equals to 3.25, the amount of brookite was the highest and reached the value of ~28.6%, while the sample of 4.5 showed only 8.6% of brookite.

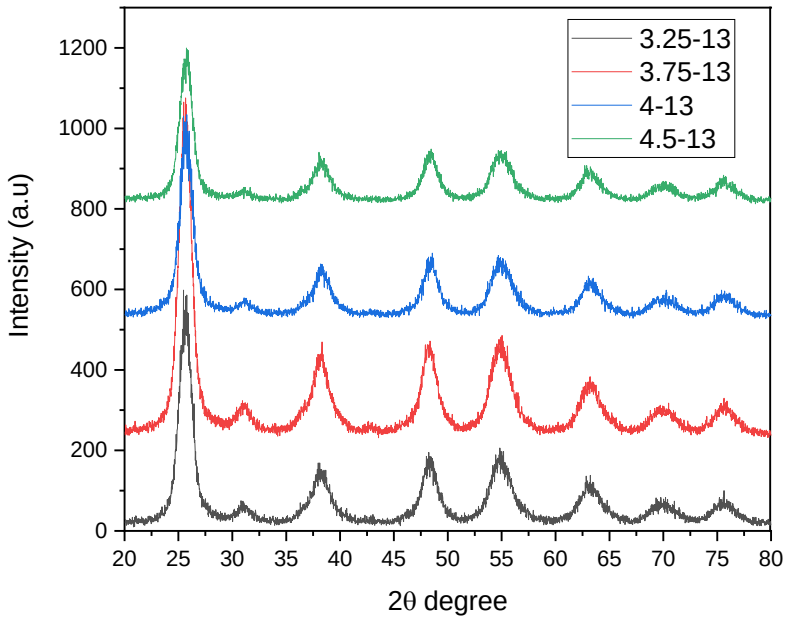

Figure 14 The XRD spectrum of different ratio of Water ot LiBr

The Raman and XRD data presented in this section show that in all 16 synthesized samples under various MSH condition, anatase and brookite phase mixture are present. We show that the amount of brookite could be controlled by changing either the water/salt or salt/TTIP molar ratio. However, the larger effect in brookite formation is associated with the amount of salt present in the MSH solution. However, our results show that both the amount of water and salt are critical parameters that can lead to a more well-defined structure in the molten salt hydrate assisted synthesis technique.

Table 3 Textural properties of different water/LiBr ratio

Sample	3.25-13	3.75-13	4-13	4.5-13
Anatase(wt%)	71.4	74.4	87.5	91.4
Brookite (wt%)	28.6	25.6	12.5	8.6

Herein, we can hypothesize the following: when water/LiBr ratio increases at fixed LiBr/TTIP molar ratio, the excess amount of water is expected to affect the first step of the sol-gel process, i.e. the hydrolysis step. The higher amount of water, the better the hydrolysis will be. In MSH, the main interaction is the ion-water interaction, cations are surrounded by water molecule in a single hydration sphere. Therefore, no excess water molecule could connect with TTIP to undergo either the hydrolysis and condensation process. However, when we increase the molar ratio of water to salt, the extra water is added in the system when we fix the salt/TTIP ratio.

Water molecules are accessible to facilitate hydrolysis and initiate the condensation process. In addition, at the extreme case of concentrated MSH medium, because of the lower ratio of water/salt compare to dilute solution, the cation of salt LiBr could serve as complexing agent, which in turn can strongly affect the second step of the sol-gel process, the condensation step. It should mention here, due to the crystal structure of anatase and brookite are composed by assembling [TiO_6] octahedral through edge-sharing and corner-sharing. For anatase each [TiO_6] is surrounded four are edge-shared and four corner-shared octahedra; for brookite each [TiO_6] is surrounded by three are edge-shared and six are corner-shared octahedra. Our hypothesis is the presence of Li^+ cation might retard or inhibit the [TiO_6] edge-shared connection in the hydrolysis process. [27-28, 63]

4.3 Effect of MSH system on the surface area and pore volume

Table 4 BET surface area and pore volume of different samples

Sample	BET surface area (m^2/g)	Pore volume (cm^3/g)
3.25-13	201	0.266
3.25-50	206	0.1312
3.25-80	114	0.0752
3.75-13	208	0.238
375-50	105	0.1684
3.75-80	143	0.0853
4-13	198	0.192
4-50	135	0.0774
4.5-13	205	0.201

Surface area and pore volume measurements have been conducted via the BET method for our samples. The data are summarized in Table 4. At fixed LiBr/TTIP ratio at 13, and water/LiBr ratio varying systematically from 3.25 to 4.5, BET surface area is always very high with its value to be around 200 m^2/g. This value is relatively high as compared to commercial TiO_2-anatase samples. A systematic decrease in surface area was observed upon increasing the LiBr/TTIP from 13 to 80 at almost all water/salt ratio. We believe that this observation might be associated with the higher amount of water which in turn increases the rate of hydrolysis. Compare to the XRD data for 3.25-13 the crystalize size is about 6 nm however it is about 9 nm for 3.25-80.

N_2 isothermal adsorption lines of samples (Fig 15), which water/salt ratio is 13, show H2 type of hysteresis loop, which demonstrate possible capillary condensation occurs in apparent mesopores. According to BET adsorption theory, H2 type represent the more complexed and less uniform pore structure. For this type, pore size distribution is wide and the pore structure is hard to determine. However, hysteresis loop for 3.25-50 and 80 are H4 type, which are totally

different from 3.25-13. According to the absorption-desorption line, at low P/P_0, samples have significant adsorption, and it does not show the absorption equilibrium plateau. This type hysteresis loop is the combination of H1 and H2 and represents the pore structure is less uniform than H2. This phenomenon usually occurs if the pore dimeter is large, typically mesopores size, and normally this pore is very narrow.

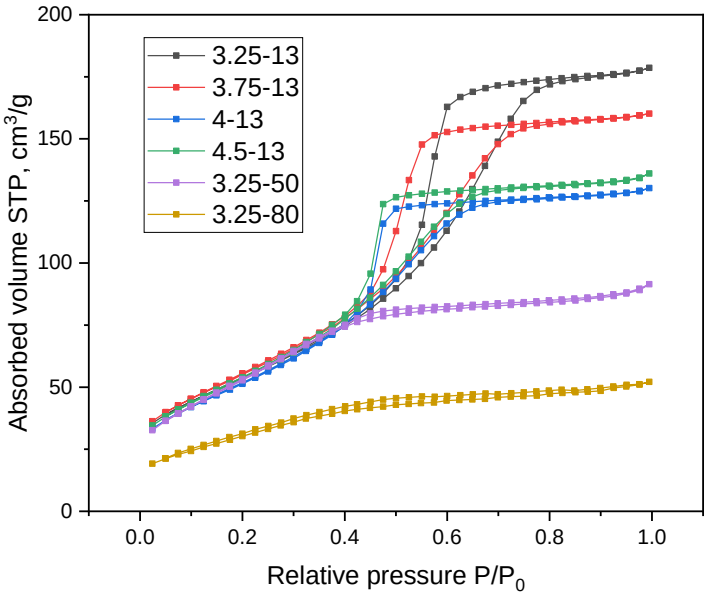

Figure 15 N_2 physisorption isotherms

4.4 Effect calcination temperature on phase transformation

The transformation of between the different crystalline phases of titanium dioxide is a process that is strongly associated with the synthesis conditions that the TiO_2 is made and is critical when one wants to control ratio of different phases. Based on thermodynamic studies, rutile is thermodynamic stable as compared to brookite and anatase. According to some researchers' kinetics studies, the anatase rutile transformation (ART) occurs at the temperature around 600 ℃; however, a wider range of transformation temperature from 400 to 1100 ℃ have been also highlighted. This phase transformation process of anatase and brookite to rutile is strongly affected by many factors, such as particle size, pH of the synthesis medium, and of course different mechanisms in various synthesis methods. However, the sequence of anatase and brookite transform to Rutile is still an ambiguous problem. Tarek A. Kandiel[29] reported the anatase changes to brookite and brookite changes to rutile, and this transformation pathway is affected by the anatase and brookite particle size and the calcination temperature.

A systemic study of ART has been conducted herein for materials synthesized in water/salt

ratio equal 3.25 and salt/TTIP ratio equal 13. In effort to find the transformation temperature, samples are calcined from the 400 ℃ to 600 ℃ with 50°C increments. Raman and XRD measurements are utilized to characterize these samples in order to unveil the temperature of each transformation.

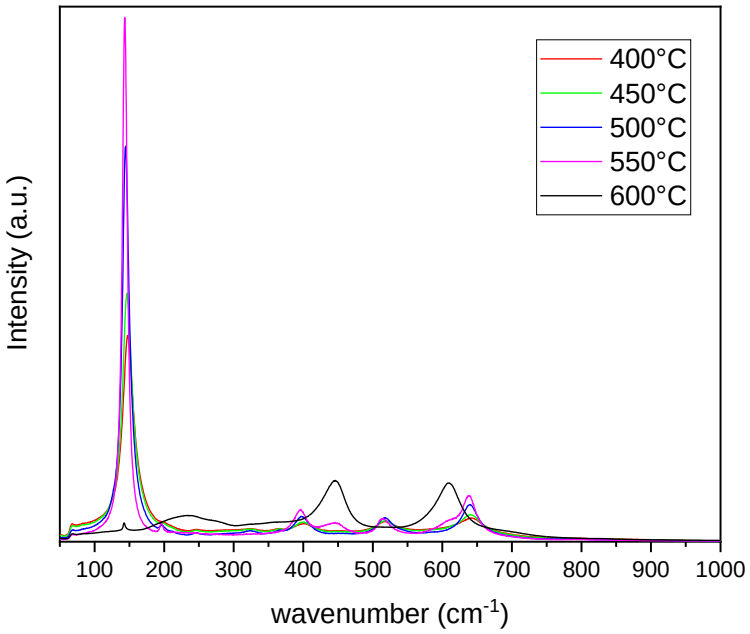

Figure 16 Raman of different calcination temperature of 3.25-13

Raman spectra of samples 3.25-13 calcined at different temperature are given in Fig 16. Anatase main peaks at 147 cm^{-1}, 399 cm^{-1}, 513 cm^{-1} and 639 cm^{-1} have a significant increase, when the calcination temperature changes from 400 to 550 ℃ indicating the clear improvement in the crystallinity of anatase phase. This follows the fact that high temperature calcination will result in an expected particle size grow. A clear peak shift from 147 cm-1 to 144 cm-1, and intensity of brookite Raman vibrational bands in 200 cm^{-1} to 300 cm^{-1} decrease significantly as observed in this process. The deconvolution approach (Fig11) shown in previous section, reveals that brookite phase is transformed to anatase phase. This result is somewhat contradictory with the literature information provided above. On the other hand, at 500 ℃ calcination temperature, two bands occur at 448 cm^{-1} and 612 cm^{-1} indicate some anatase or brookite transforms into rutile. At 600°C calcination, brookite bands are completely disappeared, and the high intensity rutile peaks obscure the whole spectral envelope. Since anatase Raman band $E_g(\nu_6)$ and rutile B_{1g} locate at same position, it is hard to distinguish whether small amount of anatase still exists in the synthesized material. Based on Raman spectra, the transformation temperature is about 550 ℃, and at 600 ℃ brookite has completely transformed to other phases. According to Raman bands of different phases growth and elimination, we suggest that the sequence of

titanium dioxide phase transformation synthesized under MSH condition follows the order: brookite to anatase and finally to rutile.

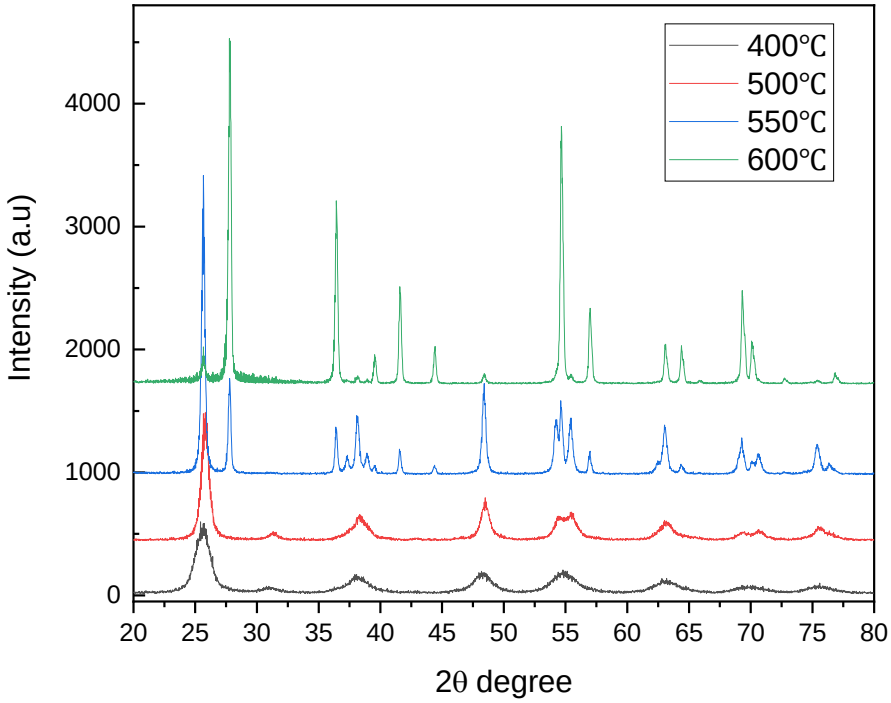

Figure 17 XRD of different calcination temperature of 3.25-13

X-ray diffraction spectra are shown in Fig 17, from 400 ℃ to 600 ℃ calcination, anatase [101] phase at 25.4 ˚(2θ) and brookite [121] phase at 30.81 ˚(2θ) are observed. However, at 550 ℃ brookite [121] phase has disappeared, which indicates the brookite has completely transformed to other phases. Meanwhile, a clear sharp peak at around 27 ˚(2θ), which is identified as rutile [110] crystal phase occurs. At 600 ℃, a small anatase [101] peak and high rutile [110] peaks are observed in the meantime. XRD spectra could complement Raman data that at higher calcination temperature there is small scale amount of anatase in the material.

Table 5 Textural properties of 3.25-13 calcined at different temperature

Temperature (℃)	Anatase(wt%)	Particle size (nm)	Brookite (wt%)	Particle size (nm)	Rutile (wt%)	Particle size (nm)
400	80.9	6	19.1	5.5		
500	90.9	13.2	9.1	18.1		
550	79.5	>100			20.5	>100
600	8.3	>100			91.7	>100

The Raman spectra and the X-ray diffraction spectra are in great agreement and highlight the possible pathway of different phases transformation of the sample 3.25-13. However, this result

is opposite to the thermodynamic study which brookite is the intermediate of anatase transforms to rutile process. We believe the difference is because of the particle size of anatase and brookite in these samples. Table 5. shows the quantity of weight percentage and the particle size of anatase, brookite and rutile in each sample. At 400 ℃, the particle size of anatase and brookite are just 6 nm and 5.5 nm. Zhang reported that the particle size could affect the thermodynamic stability of anatase and brookite. They concluded that the stable particle size range of anatase, brookite and rutile is <11nm, 11nm-35nm, >35nm individually. At low calcination temperature the anatase particles appear to have an average size around 6 nm; however, brookite particle size is lower than 11nm. Therefore, brookite transforms to the anatase firstly. At higher temperature, since anatase particle size is much larger than 11nm, anatase become more unstable and transforms to Rutile finally.

4.5 Acidity measurements via TPD-MS

Acid sites play important role in catalysis, for instance Velisoju[57] reported the Ni/TiO_2 performs high selectivity towards γ-valerolactone (GVL) due to the Lewis acid site on material. Since TiO_2 has the potential to possess both Lewis and Bronsted acid sites, understanding the acidity of our materials is considered important if one takes into account its potential in the catalysis field. MA Aramendí[58] reported that pyridine is able to adsorb on the Lewis acid site and Bronsted acid site, while the 2,6-dimethylpyridine could only adsorb on Bronsted acid site. Thus, to characterize and quantify Lewis acid and Bronsted acid sites by using two different types of pyridine Temperature-Programmed-Desorption (TPD)-MS respectively has been accomplished.

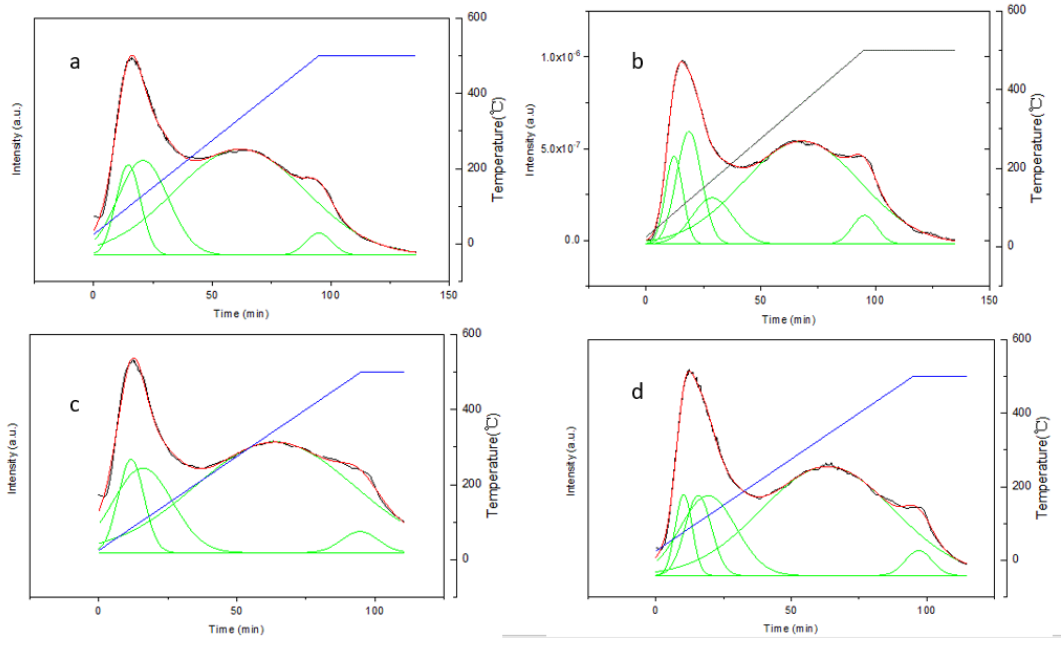

Figure 18 Pyridine TPD-MS of 3.25-13 (a), 3.75-13 (b), 4-13 (c) and 4.5-13 (d)

The deconvolution of pyridine TPD-MS of water/salt ratio form 3.25-4.5 with the salt/water ratio is 13 are shown in Fig 18. These four samples display pyridine desorption with temperature increase from 25 to 500℃ with the 5℃/min ramping. A huge asymmetric desorption peak occurs below 200℃ for these four samples. After then a wide peak occurs at about 60 mins when the temperature is about 320℃. Another small desorption peak at around 90 to 100 mins when the temperature is around 480℃. Pyridine TPS-MS data indicate that TiO_2 materials synthesized under MSH condition possess both Lewis acid sites and Bronsted acid sites. Normally, the peaks appear below 200 ℃ are associated with weak acids, from 200 to 400 ℃ have medium strength while at higher than 400 ℃ strong acid site are present. Based on the 2,6-dimethylpyridine TPD-MS (Fig 19), a huge peak occurs at the low temperature (around 200℃), which is similar to pyridine TPD-MS in this temperature range. Compare with the 2,6-dimethylpyridine TPD-MS (Fig 19), and since 2,6-dimethyl pyridine could only be adsorbed on Bronsted acid, we conclude that the huge peak at low temperature belongs to weak Bronsted acid sites. The deconvolution of pyridine and 2,6-dimethylpyridine depicts that these multiple Bronsted acid sites, different in nature, may exist simultaneously. One can hypothesize that the reason behind the multiple Bronsted acid sites can be associated with the increased hydroxylation of the TiO_2 surface. Considering also that different extent as well as nature of hydroxylation may occur between anatase and brookite it is expected that various weak Bronsted acids may exist. At higher temperature (above 200℃), a huge peak (at around 330℃) and a small peak (at 480℃) arise which belong to Lewis acid sites. Deconvolution of pyridine and 2,6-dimethylpyridine TPD-MS expresses Lewis acid sites are stronger than Bronsted acid sites. This is because, as mentioned above, the Bronsted acid sites are some hydroxyl group on the surface of TiO_2 (Ti-OH). However, the Lewis acid sites are Ti^{4+} cation exposed on the surface. At higher temperature, the bond of Ti-OH will break, but Ti^{4+} cation is much stable on the surface[51].

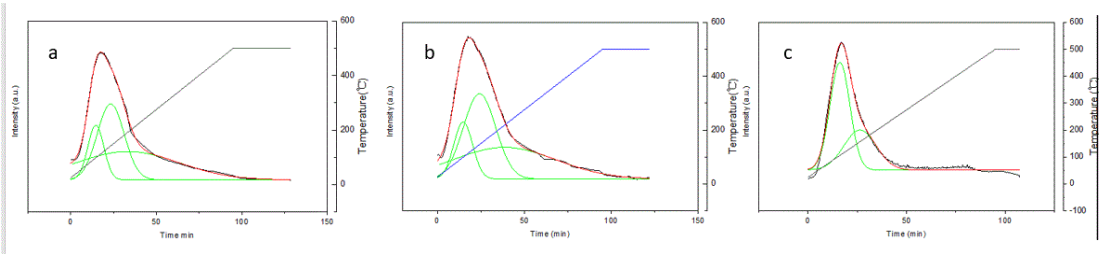

Figure 19 2,6-dimethyl pyridine TPD 3.25-13(a), 3.75-13 (b) and 4-13 (c)

After the calibration of pyridine TPD-MS, the amount of the acid site of the 3.75-13 and 3.25-50 is 0.2396 and 0.216 mmol/g. Compare to the values with methods synthesized TiO_2 (Table 6). It is safe to say the amount of the acid site MSH TiO_2 is higher than $TiCl_4$ precipitation,

commercial P25 and sol-gel titanium *n*-butoxide.

Table 6 Amount of acid sites of different samples compare to lecture

Sample	3.75-13	3.25-50	$TiCl_4$ Precipitation[60]	Commercial P25[61]	Sol-gel titanium *n*-butoxide[62]
Amount of acid sites (mmol/g)	0.2396	0.216	0.161	0.18	0.1727

4.6 Morphology of MSH assisted TiO_2

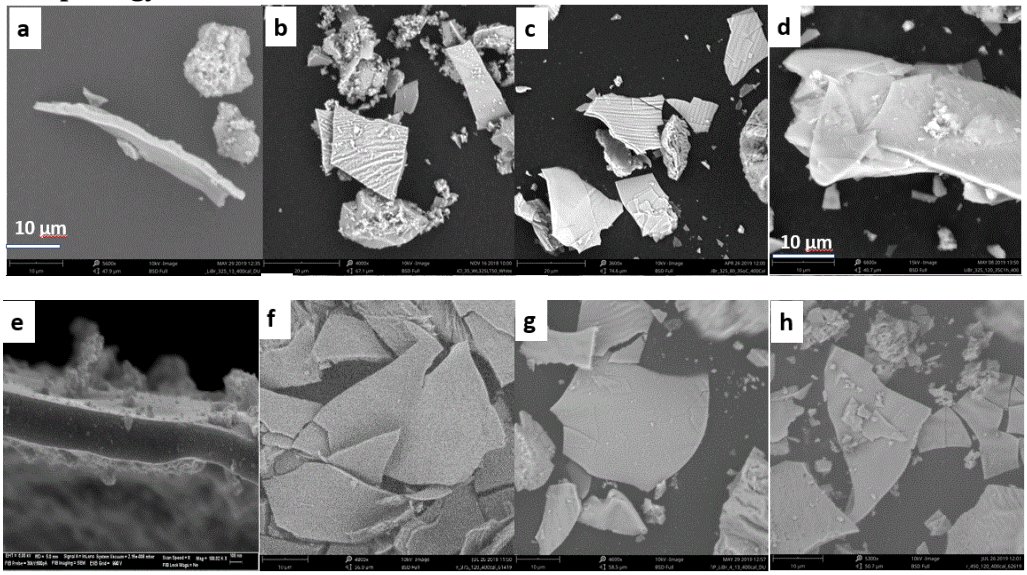

Figure 20 SEM images of TiO2 (a) 3.25-13, (b) 3.25-50, (c) 3.25-80, (d) 3.25-120, (e) 3.75-13, (f) 3.75-120, (g) 4-80, (h) 4.5-120

SEM images of MSH TiO_2 are shown in Fig 20. As it shown in these pictures, morphology of MSH TiO_2 displaces 2D flake like structure. A closer look of images from a-d, the flake like morphologies of samples 3.25-13 to 3.25-120 are irregular shape and the thickness of this 2D flake like structure has a clear decrease. Comparing with other water/salt ratio samples, this thickness decreasing trend always occur when salt/TTIP ratio increase. This result reveals that the amount of water in MSH system might be responsible for the morphology control.

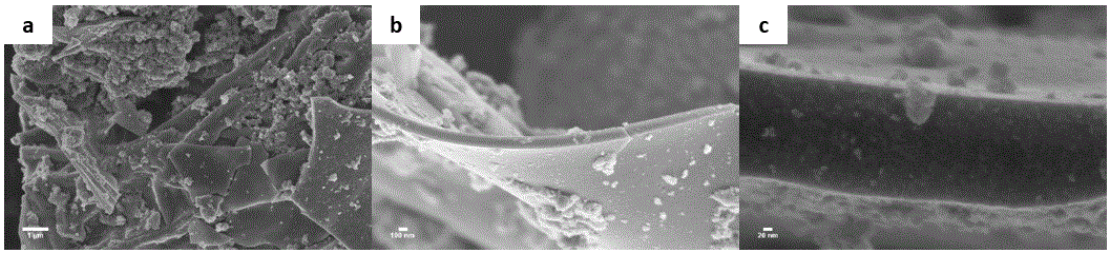

Figure 21 High-resolution SEM micrographs of the TiO_2 prepared at a H2O/LiBr ratio equal to 3.75 at different level of magnification. Scale bars at (a) 1 µm, (b) 100 nm, and (c) 20 nm

High resolution SEM images of water/LiBr ratio equal to 3.75 are shown in Figure 21. Some small sphere particles on flake like surface could be clearly observed. The scale of these particles is about 5-10 nm contrast to more than 100 nm thickness flake. Focusing on these small particles on flake surface, we could hypothesize that the flake like structure comes from the agglomeration or reorganization of these small particles. However, in the molten salt hydrates medium due to the low interaction between water-water, hydrolysis and condensation of sol-gel has been retard, which prohibits this ordered agglomeration of small particles.

4.7 Effect of aging time on the Raman spectra of TiO_2 samples

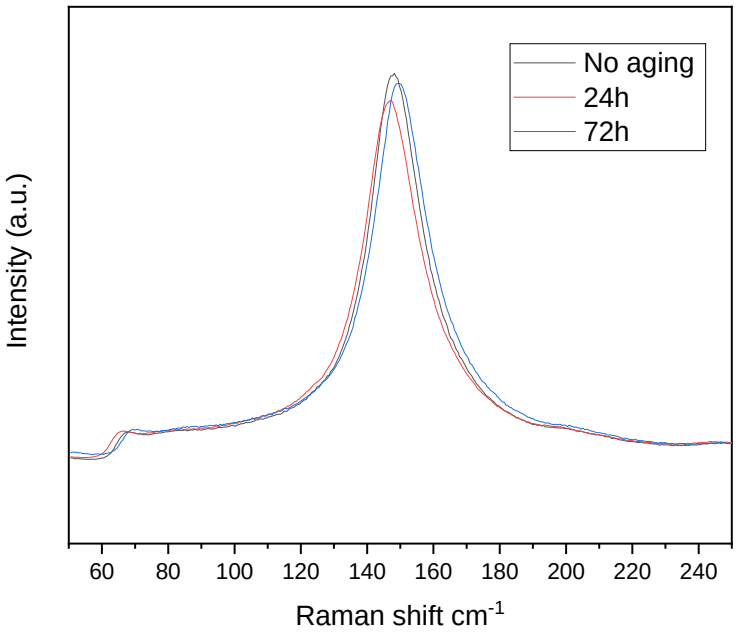

Figure 22 3.25-13 with different aging time

Aging time is an important factor to affect the synthesized material. Zhang [63]reported that the aging time could affect the mesoporosity of nanocrystalline materials. They discovered that phase transformation temperature of TiO_2 can decrease about 100℃ when the sample is treated for longer aging time. Therefore, it is necessary to study how the aging time affects our samples.

The sample with water/salt ratio 3.25 and salt/TTIP ratio 13 is prepared with no aging time, 24h, and 72h aging time. Based on Raman spectra (Fig 22) of these three samples, when no aging process was followed, the Eg band of anatase appears highly symmetric which is characteristic of a material with mainly one phase. Upon increasing aging time, slight shoulder to higher frequency is observed which might be indicative of the presence of brookite. However, more systematic spectroscopic analysis together with XRD measurements can shed more light

into the actual effect of aging time on the molecular structure as well as crystallinity of our samples.

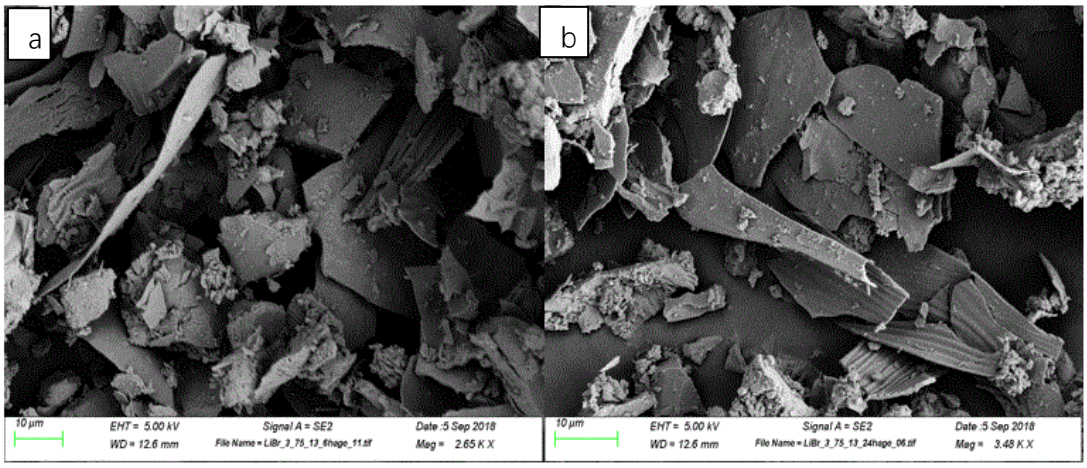

Figure 23 FESEM images of 3.75-13 aging (a) 6 h, (b) 24 h

In an effort to investigate the possible morphological changes by dealing with different aging time, FESEM images of the sample 3.75-13 with 6 h and 24 h aging time are shown in Fig 23. By comparing the SEM image of 3.75-13 (Fig 20 e, no aging) in the previous part with those reported in Figure 23 it is observed that increasing the aging of materials more flake like morphologies observed. This behavior is believed to arise from the longer condensation time present. As discussed above, sol-gel method has two processes the first step occurs immediately as the precursor is added in solution. Whereas, the condensation process occurs via dehydration from the metal hydroxide network to the final metal oxide. This process might be slower than hydrolysis. One-hour reaction maybe too short for the particles to growth in MSH. Therefore, longer aging time provides particles more time to growth in the condition. Interestingly, they do not lose the flake-like morphology. Another evidence is the texture of one-hour reaction samples are much more loose compare to long time aging samples. Therefore, it is easy to deduce that aging time might play a very important factor to affect the properties of samples. Consequently, adjusting the aging time, it is possible to control the morphology and crystal particle size of the TiO_2 materials prepared in MSH reaction media.

4.8 Effect of basic conditions in the MSH synthesis of TiO_2

The presence of basic conditions in the synthesis process might affect the nucleation of TiO_2, which in turn might change crystalline phase, morphology and thermostability. In order to understand this effect in MSH synthesis TiO_2, 3.25-13 (water/salt-salt/TTIP) was synthesized in the presence of NH_4OH. Before adding the ammonium hydroxide, the pH of the solution is

about 5.2, after adding 2 ml ammonium the pH increases to about 6.29. The materials prepared in the presence of NH_4OH were calcinated at four different temperatures, 400℃, 600℃, 700℃ and 800℃. Surprisingly, as the Raman spectra indicate, brookite peaks in the range of 200 to 350 cm^{-1} are not observed (Fig 24); whereas, anatase Raman peaks are clearly seen. Interestingly we observe that in the presence of NH_4OH, even at 600℃ the main crystalline phase observed was anatase as oppose to rutile in the absence of NH_4OH (shown earlier). It is known that sol-gel methods usually lead to less crystalline material. However, it seems herein that NH_4OH can improve the crystallinity as well as thermal stability of TiO_2 materials. At 700℃ calcination temperature, clear decrease of anatase peaks and at 235cm^{-1}, 488 cm^{-1} and 612 cm^{-1} represent large part of anatase phase transforms to rutile phase. At 800℃ calcination temperature the anatase Raman vibrational bands have already disappeared and only the rutile peaks can be seen.

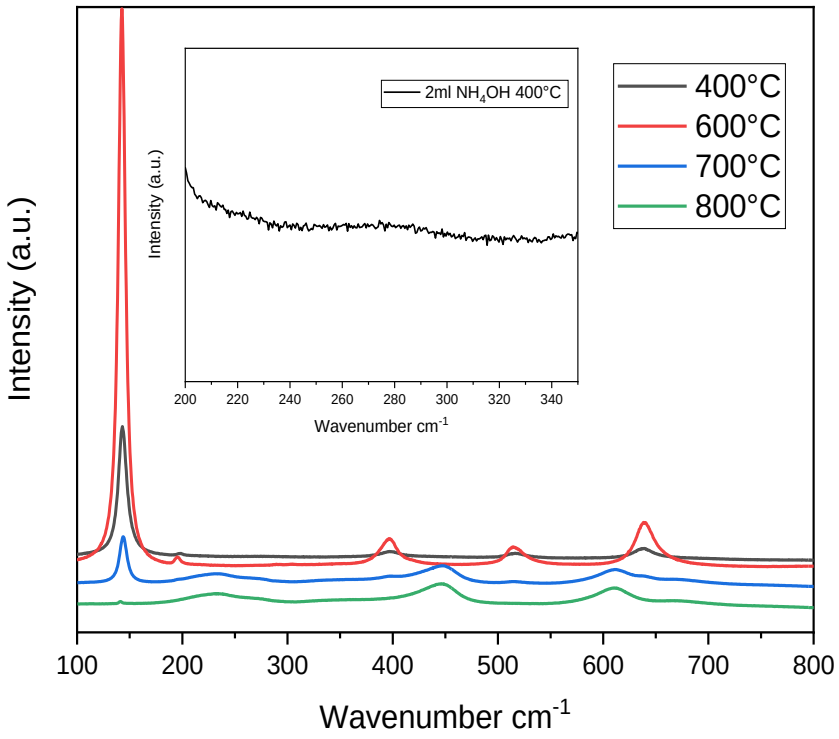

Figure 24 3.25-13 with 2ml NH_4OH

Based on the Raman results NH_4OH could not only control the TiO_2 crystalline phases towards more anatase, but also improve the thermal stability of single anatase phase. The ART temperature was increased abaroundout 100 ℃. In the process where NH_4OH was used, TiO_2 brookite phase was not detected by means of Raman spectroscopy, which is opposite to some researchers' that shown the transformation routine to follow the order of anatase to brookite and to rutile. MSH synthesized ammonium TiO_2 transformed from anatase to rutile directly. The morphology (Fig 25 b) of the ammonium added TiO_2 sample shows the totally different

structures compare with the previous same ratio samples. No flake like morphology occur in ammonium TiO_2.

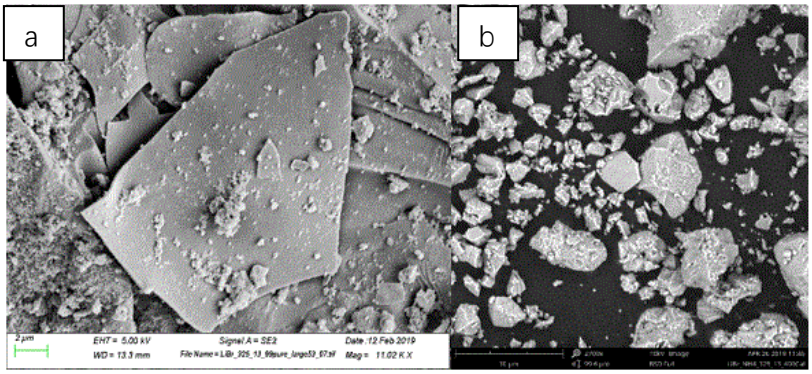

Figure 25 3.25-13 (a) Without NH_4OH (b) with NH_4OH

As discussed before, the presence of NH_4OH changes the morphology and thermostability of MSH TiO_2. We believe that the reason behind this is associated with the hydrolysis ratio. Each phase TiO_2 could be considered as lots of $[TiO_6]$ octahedral assembled by connecting via edge-shared and corner-shared units. For anatase each $[TiO_6]$ is surrounded by 8 octahedra, which four are edge-shared and four are corner-shared; for rutile each $[TiO_6]$ is surrounded 10 octahedra, tow are edge-shared and eight are corner-shared; for brookite each $[TiO_6]$ is surrounded by nine octahedra, three are edge-shared and six are corner-shared[23,28,63]. During this process, Ti^{4+}-hydrated octahedral monomer plays a very important role in the nucleation process[24]. Ti^{4+}-hydrated octahedral monomer could be represent as $[Ti(OH)_h(H_2O)_{6-h}]^{4-h}$, here h is the hydrolysis ratio. The $[Ti(OH)_h(H_2O)_{6-h}]^{4-h}$ octahedral monomers have two bonds, one is h Ti-OH, and other bond is (6-h) Ti-H_2O. In the condensation process, one water molecule will be removed in this process. This condensation of octahedral monomers follows two reactions: Olation and oxolation. [28,63]

Olation: Ti-OH + Ti-H_2O → Ti-OH-Ti+H_2O

Oxolation： Ti-OH+Ti-OH→Ti-O-Ti+ H_2O

These two different reactions are determined by the number of Ti-OH bond and Ti-H_2O bond. Therefore, the hydrolysis ratio h is the most important factor. This hydrolysis ratio could be calculated by using the following equation.[28]

$h = (1.0584 + 0.3181\ pH)/(0.6794 + 0.01776\ pH)$

There are three important value of this h. If the h <2, the rutile phase is crystallized; 2< h <3,

the crystallization is the mixture of rutile, brookite or anatase phases; if 3< *h* <5, anatase phase is crystallized; 5< *h*, brookite is crystallized.

After added the 2 ml NH_4OH, the pH of the solution is about 6.29. The hydrolysis ratio h can be calculated by equation is equal to 3.8, which is in the range of 3< *h* <5. Therefore, only anatase phase is crystallized. We believe that by changing the pH of solution system to modify hydrolysis ratio can modified the phase in MSH TiO_2; however, the presence of NH_4OH does not lead to the formation of flake-like materials which is probably associated with the hydrolysis ratio change.

4.9 Effect of MSH synthesis conditions on the band gap energy of TiO_2

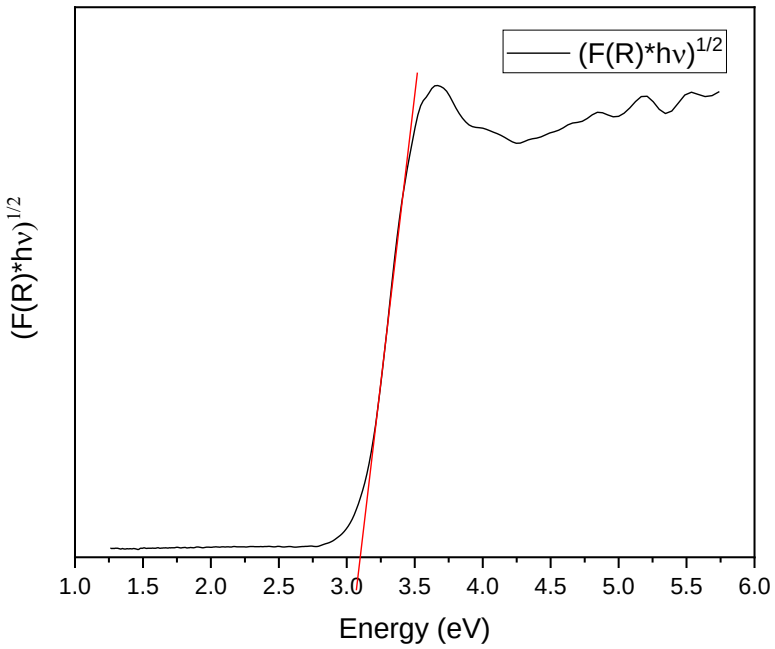

Figure 26 K-M method of 3.25-13 band gap energy

As one of the most important semiconductor materials, band gap energy of synthesized TiO_2 materials under MSH condition has been by using UV-vis spectroscopy. We compared samples, which were synthesized with a fixed ratio of salt/TTIP and varied ratio of water/LiBr. Both Tauc method and differential diffuse-reflectance UV-vis spectroscopy method was utilized for the analysis of bandgap energy of these materials Using Tauc method for direct allowed transition bandgap, we report a bandgap energy for 3.25-13 sample as 3.1 eV.

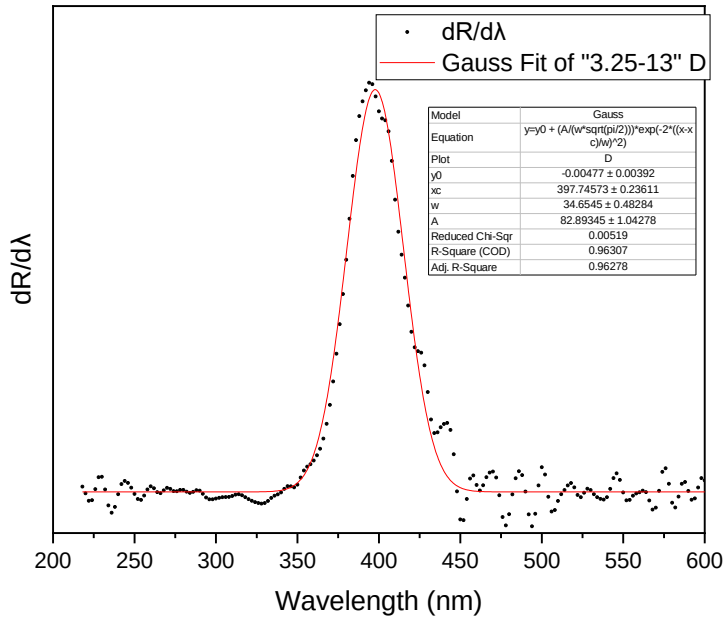

Figure 27 DPR method of 3.25-13 band gap energy

Fig 27 describes the DPR method to quantify the band gap energy of 3.25-13. Plotting the diffusion reflectance UV-vis data after treated by differential, then after using the gaussian function to fit the scattered data, the center of the peak represents the wavelength of the light which is absorbed by semiconductor materials. Calculating the band gap energy by using the equation (2) is 3.12eV of 3.25-13, which is much similar to the value of we obtained by the Tauc method. Table 7 displays synthesized materials and the commercial titanium dioxide anatase, brookite and rutile. The key point should be mentioned here is the DPR method could not distinguish the direct or indirect band gap. The exactly information of band gap of materials should be calculated by DFT computational chemistry.

Table 7 Band gap energy of different ratio of water/LiBr and commercial titanium dioxide

Metal oxide	K-M method BGE (eV)	DPR method BEG (eV)	Reference BEG (eV)
Anatase	3.33	3.25	3.2
Brookite	3.41	3.33	3.27
Rutile	3.09	3.14	3.03
3.25-13	3.1	3.12	
3.75-13	3.11	3.14	
4-13	3.05	3.09	
4.5-13	3.08	3.1	

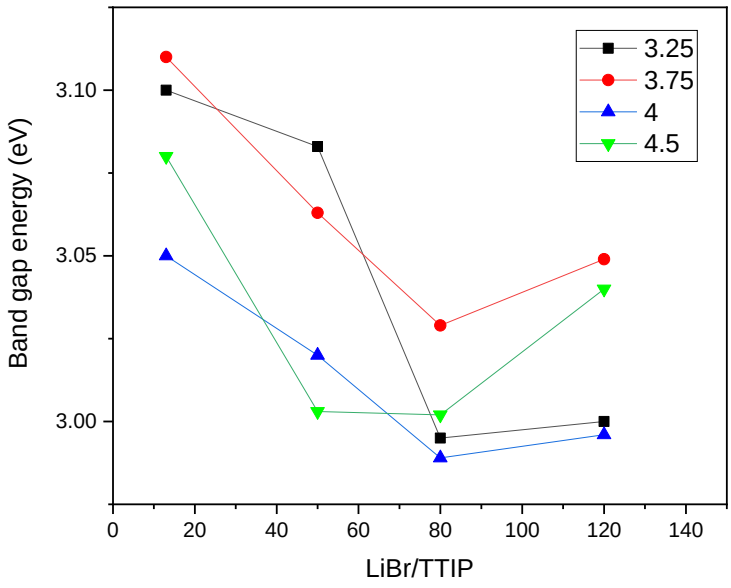

Figure 28 Band gap energy of all materials

The other samples' band gap energy calculated by Tacu method have shown in Fig 28. Band gap energy of samples synthesized under MSH are much lower than the pure commercial anatase and brookite. A similar trend of band gap energy change can be observed. Bandgap energy seem to experience no effect by changing water/salt ratio and tended to decrease as the salt/TTIP ratio increase from 13-80. Due to this band gap variation trend, MSH might become a reliable method to control band gap by changing the salt/TTIP ratio. There are many factors might affect this property, such as materials and synthesis method. One hypothesis might explain the unique trend of band gap energy is the quantum confinement effect. The main principle of this theory is that the band gap energy is correlating to the particle scale.

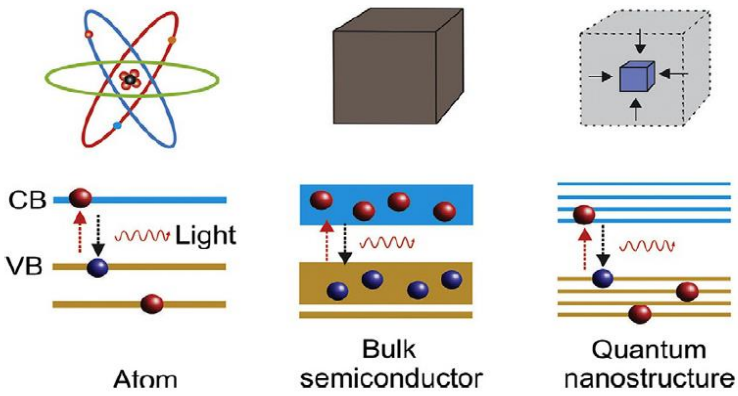

Figure 29 Energy band gap in atom, bulk and quantum nanostructure[56]

Quantum structure could be defined by the number of reduced dimensions, or the number of

degrees of freedom experienced by electrons and holes inside the material. Traditionally, quantum structure could be divided quantum well (2D), quantum wire (1D) and quantum dot (0D), while bulk could be considered 3D structure (shown in Fig 19). Generally, for the 2D, 1D or 0D structures, the electrons movement are limited by their structure. For instance, in the 2D structure quantum well, electrons are only move in two directions compare to bulk. However, for the bulk size, electrons are free to move in all directions. In this structure, all electron levels are squeezed that result in the ban gap energy of bulk structure is much lower than other structures[56]. Therefore, when the material size increases the band gap decrease. This theory best explains the materials whose particle size especially below 10 nm. This quantum confinement theory could successfully explain the trend of band gap energy when the salt/TTIP ratio increase from 13 to 80. Brookite and anatase particle size of samples, which were synthesized with fixed water/salt ratio (3.25) and various salt/TTIP ratio (from 13 to 120), were calculated from XRD data as shown in Table 8. According to XRD data, brookite particle size increases from 3.7 nm to 9.5 nm, while the anatase particle size does not change significantly in the salt/TTIP ratio range from 13-80. Herein, the increase of brookite particle size is contribute to band gap energy decrease. However, this theory could not account for the increase of band gap when the salt/TTIP ratio is 120. Due to the quantum confinement theory, as anatase particle size has a significant increase from 6.4 nm to 9 nm, the band gap energy should keep decreasing, however it is not observed. This problem requires more deep study.

Table 8 Band gap energy of 3.25 with different salt/TTIP ratio and particle size

LiBr/TTIP	Band gap energy (eV)	Brookite particle size (nm)	Anatase particle size (nm)
13	3.1	3.7	6.1
50	3.083	9.4	6.8
80	2.995	9.5	6.4
120	3	9.5	9

5. Future work

TiO_2 is very important semiconductor and has been widely applied in photocatalysis. According to our UV-vis data shown earlier, the band gap energies of our samples (between 3.1-3 eV) are lower than the commercial anatase (3.3 eV) and brookite (3.4 eV). Therefore, it is very necessary to try these materials in the photocatalysis.

Water splitting reaction is a very important reaction that can occur photocatalytically to produce hydrogen from water. However, two challenges in the photocatalysis exist. One of that is that the band gap of TiO_2 is highe, thus it only has activity in ultraviolet radiation. Another limitation is the undesired electron hole back reaction. There are two ways to improve the photocatalytic activity. The first method is by loading metal atoms on the surface TiO_2. The excited electrons on the conduction band could move on the metal, in this way we could inhibit the electron-hole back reaction. Reduction will happen on the metal, and oxidation will happen on the semiconductor valence band. Another method is by utilizing sacrificial reagents. This kind of sacrificial reagent, also called electron donors or electron acceptor scavenger. The electron donor could react with the hole on valence band; thus, the photo efficiency could be improved. Another advantage is some sacrificial reagents could serve as reactants to improve the yield of the hydrogen.

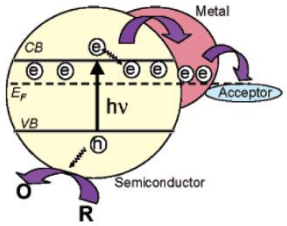

Figure 30 Mechanism of loading metal

There are lot of sacrificial reagents, like methanol, EDTA and Na_2S. Since methanol is low cost as well as it could serve as a reactant, thus methanol is the first choose for sacrificial reagent. The mainly process has three steps:

$CH_3OH \rightarrow HCHO + H_2$

$HCHO + H_2O \rightarrow HCO_2H + H_2$

$HCO_2H \rightarrow CO_2 + H_2$

For our sample, it has two advantage. Firstly, the band gap energy is lower than commercial anatase. Secondly, for some materials, they have much higher surface area (about 200 m^2/g). Thus, future efforts can be placed on loading some metals like Pt, Ag to improve the photocatalytic efficiency.

6. Conclusions

Due to the great advantages and wide applications of TiO_2, the investigation of a new synthesis method to produce high quality TiO_2 is research topic of prime interest to academia. In this work, we report that the molten salt hydrate assisted sol-gel method to synthesize TiO_2 provides great enhancements. Our fundamental hypothesis is that, under the molten salt hydrate condition, the water-water interactions are minimized, thereby retarding the hydrolysis or condensation rates of TTIP, which prohibits the bulk agglomeration of small particles. Using these special conditions to synthesize titania, MSH TiO_2 exhibits unique properties. Anatase and brookite mixed phases were observed in MSH TiO_2. Also, ratios of water/salt (from 3.25 to 4.5) and salt/TTIP (13 to 120) are important parameters to control compositions of material. At higher salt/TTIP ratio, the amount of brookite decreases, and materials become more crystalline. 2D flake-like morphologies of materials are observed by SEM technology. Another interesting point is that the thickness of flake structure could be controlled by changing salt/TTIP ratio. Varying aging time does not change compositions, however, with long aging time, materials might have more flake-like morphology, which we surmise is because the aging process might extend condensation time. The basic condition of molten salt hydrates could change the condensation pathway by changing the hydrolysis ratio. Under high pH condition, only anatase phase and irregular particle morphology could be observed. However, high crystalline and thermostable anatase was synthesized under this condition. High surface area, large amount of acid sites and low band gap energy were likewise some unique properties of MSH TiO_2 observed by multiple techniques. The unique band gap energy trend of MSH TiO_2 was discovered. We believe this decreasing trend might be because of quantum confinement. Finally, the unique anatase-rutile transformation (ART) pathway of MSH TiO_2 was discovered. This phenomenon could be explained by particle size effect. Due to the enhancement of TiO_2 properties afforded by MSH-assisted synthesis, we believe that this method will prove to be advantageous for future research and industrial application.

References

[1] Hagen, J., 2008. *Industrial Catalysis*. Weinheim: Wiley-VCH.

[2] Thomas, J. and Thomas, W., 1997. *Principles And Practice Of Heterogeneous Catalysis*. Weinheim [etc.]: VCH.

[3] Knözinger, H., & Kochloefl, K. (2003). Heterogeneous Catalysis and Solid Catalysts. *Ullmann's Encyclopedia of Industrial Chemistry*.

[4] Manna, P., Debgupta, J., Bose, S., & Das, S. K. (2016). A Mononuclear CoII Coordination Complex Locked in a Confined Space and Acting as an Electrochemical Water-Oxidation Catalyst: A "ship-in-a-Bottle" Approach. *Angewandte Chemie - International Edition*, *55*(7), 2425–2430.

[5] B. C. Gates: *Catalytic Chemistry*, Wiley, New York, 1992.

[6] C. N. Satterfield: *Heterogeneous Catalysis in Industrial Practice*, McGraw-Hill, New York, 1991.

[7] Schlögl, R. (2015). Heterogeneous catalysis. In *Angewandte Chemie - International Edition* (Vol. 54, Issue 11).

[8] Takenaka, S., Kobayashi, S., Ogihara, H., & Otsuka, K. Ni/SiO2 catalyst effective for methane decomposition into hydrogen and carbon nanofiber. *Journal of Catalysis*, (2003). *217*(1), 79–87.

[9] Li, F. B., & Li, X. Z. The enhancement of photodegradation efficiency using Pt-TiO2 catalyst. *Chemosphere*, (2002). *48*(10), 1103–1111.

[10] Bal, R., Tada, M., Sasaki, T., & Iwasawa, Y. Direct phenol synthesis by selective oxidation of benzene with molecular oxygen on an interstitial-N/Re cluster/zeolite catalyst. *Angewandte Chemie - International Edition*, (2006). *45*(3), 448–452.

[11] Orita, H., Uchida, K., & Itoh, N. Adsorption of thiophene on an MoS2 cluster model catalyst: Ab initio density functional study. *Journal of Molecular Catalysis A: Chemical*, (2003). *193*(1–2), 197–205.

[12] Kibsgaard, J., Lauritsen, J. V., Lægsgaard, E., Clausen, B. S., Topsøe, H., & Besenbacher, F. Cluster-support interactions and morphology of MoS2 nanoclusters in a graphite-supported hydrotreating model catalyst. *Journal of the American Chemical Society*, (2006). *128*(42), 13950–13958.

[13] Masao Sato, Tatsumi Kanbayashi, Norio Kobayashi,etc. Hydroxyl Groups on Silica, Alumina, and Silica-Alumina Catalysts. *Journal of catalysis*, (1967). *351*, 342–351.

[14] Harima, Y., Fujita, T., Kano, Y., Imae, I., Komaguchi, K., Ooyama, Y., & Ohshita, J. Lewis-acid sites of TiO2 surface for adsorption of organic dye having pyridyl group as anchoring unit. *Journal of Physical Chemistry C*, (2013). *117*(32), 16364–16370.

[15] Cavallaro, S. Ethanol Steam Reforming on Rh/Al2O3 Catalysts. *Energy and Fuels*, (2000). *14*(6), 1195–1199.

[16] Height, M. J., Pratsinis, S. E., Mekasuwandumrong, O., & Praserthdam, P. Ag-ZnO catalysts for UV-photodegradation of methylene blue. *Applied Catalysis B: Environmental*, (2006). *63*(3–4), 305–312.

[17] Ernst, B., Libs, S., Chaumette, P., & Kiennemann, A. Preparation and characterization of Fischer-Tropsch active Co/SiO2 catalysts. *Applied Catalysis A: General*, (1999). *186*(1–2), 145–168.

[18] Cao, L., Gao, Z., Suib, S. L., Obee, T. N., Hay, S. O., & Freihaut, J. D. Photocatalytic oxidation of toluene on nanoscale TiO2 catalysts: Studies of deactivation and regeneration. *Journal of Catalysis*, (2000). *196*(2), 253–261.

[19] Ponzi, M., Duschatzky, C., Carrascull, A., & Ponzi, E. Obtaining benzaldehyde via promoted V2O5 catalysts. *Applied Catalysis A: General*, (1998). *169*(2), 373–379.

[20] Du Soung Kim, Jean-Michel Tatibouet, Israel E.Wachs. Surface structure and reactivity of CrO3/SiO2 catalysts. *Journal of Catalysis* (1992). 209–221.

[21] Eon, J. G., Olier, R., & Volta, J. C. Oxidative dehydrogenation of propane on γ-Al2O3 supported vanadium oxides. In *Journal of Catalysis*, (1994). 145(2), 318–326.

[22] Sato, Y., Aoyama, T., Takido, T., & Kodomari, M. Direct alkylation of aromatics using alcohols in the presence of NaHSO4/SiO2. *Tetrahedron*, (2012). *68*(35), 7077–7081.

[23] Chen, X., & Mao, S. S. Titanium dioxide nanomaterials: Synthesis, properties, modifications and applications. *Chemical Reviews*, (2007). *107*(7), 2891–2959.

[24] Ranjit, K. T., & Viswanathan, B. Synthesis, characterization and photocatalytic properties of iron-doped TiO2 catalysts. *Journal of Photochemistry and Photobiology A: Chemistry*, (1997). *108*(1), 79–84.

[25] Maira, A. J., Yeung, K. L., Lee, C. Y., Yue, P. L., & Chan, C. K. Size effects in gas-phase photo-oxidation of trichloroethylene using nanometer-sized TiO2 catalysts. *Journal of Catalysis*, (2000). *192*(1), 185–196.

[26] Haggerty, J. E. S., Schelhas, L. T., Kitchaev, D. A., Mangum, J. S., Garten, L. M., Sun, W., Stone, K. H., Perkins, J. D., Toney, M. F., Ceder, G., Ginley, D. S., Gorman, B. P., & Tate, J. High-fraction brookite films from amorphous precursors. *Scientific Reports*, (2017). *7*(1), 1–11.

[27] Kumar, S. G., & Rao, K. S. R. K. Polymorphic phase transition among the titania crystal structures using a solution-based approach: From precursor chemistry to nucleation process. *Nanoscale*, (2014). *6*(20), 11574–11632.

[28] Zhang, J., Sun, P., Jiang, P., Guo, Z., Liu, W., Lu, Q., & Cao, W. The formation mechanism of TiO2 polymorphs under hydrothermal conditions based on the structural evolution of

[Ti(OH)h(H2O)6-h]4-h monomers. *Journal of Materials Chemistry C*, (2019). *7*(19), 5764–5771.

[29] Kandiel, T. A., Robben, L., Alkaim, A., & Bahnemann, D. Brookite versus anatase TiO2 photocatalysts: Phase transformations and photocatalytic activities. *Photochemical and Photobiological Sciences*, (2013). *12*(4), 602–609.

[30] Galińska, A., & Walendziewski, J. Photocatalytic water splitting over Pt-TiO2 in the presence of sacrificial reagents. *Energy and Fuels*, (2005). *19*(3), 1143–1147.

[31] Zhipeng Huang, Zhitong Zhao, Chaofeng Zhang, Jianmin Lu, Huifang Liu, Nengchao Luo, Jian Zhang, Feng Wang. Enhanced photocatalytic alkane production from fatty acid decarboxylation via inhibition of radical oligomerization. *Nature Catalysis*, 2020(3), 170–178.

[32] Ilkeun Lee, Ji Bong Joo, Yadong Yin,etc. A Yolk@Shell Nanoarchitecture for Au/TiO2 Catalysts. *Angewandte chemie*, 2011(50), 10208-10211.

[33] Takanabe, K., Nagaoka, K., Nariai, K., & Aika, K. I. Influence of reduction temperature on the catalytic behavior of Co/TiO2 catalysts for CH4/CO2 reforming and its relation with titania bulk crystal structure. *Journal of Catalysis*, (2005). *230*(1), 75–85.

[34] López, R., & Gómez, R. Band-gap energy estimation from diffuse reflectance measurements on sol-gel and commercial TiO2: A comparative study. *Journal of Sol-Gel Science and Technology*, (2012). *61*(1), 1–7.

[35] Isley, Sara L., Penn, Lee R. Relative brookite and anatase content in sol-gel-synthesized titanium dioxide nanoparticles, 2006 *110*(31), 15134-15139.

[36] MacWan, D. P., Dave, P. N., & Chaturvedi, S. A review on nano-TiO2 sol-gel type syntheses and its applications. *Journal of Materials Science*, (2011). *46*(11), 3669–3686.

[37] Bischoff, B. L., & Anderson, M. A. Peptization Process in the Sol-Gel Preparation of Porous Anatase (TiO2). *Chemistry of Materials*, (1995). *7*(10), 1772–1778.

[38] Oskam, G., Nellore, A., Penn, R. L., & Searson, P. C. The growth kinetics of TiO2 nanoparticles from titanium(IV) alkoxide at high water/titanium ratio. *Journal of Physical Chemistry B*, (2003). *107*(8), 1734–1738.

[39] Reddy, B. M., Khan, A., Yamada, Y., Kobayashi, T., Loridant, S., & Volta, J. C. Structural characterization of CeO2-TiO2 and V2O5/CeO2-TiO2 catalysts by Raman and XPS techniques. *Journal of Physical Chemistry B*, (2003). *107*(22), 5162–5167.

[40] Chimentão, R. J., Medina, F., Fierro, J. L. G., Llorca, J., Sueiras, J. E., Cesteros, Y., & Salagre, P. Propene epoxidation by nitrous oxide over Au-Cu/TiO2 alloy catalysts. *Journal of Molecular Catalysis A: Chemical*, (2007). *274*(1–2), 159–168.

[41] Wang, Z., Wang, G., Louis, C., & Delannoy, L. Novel non-noble bimetallic Cu-Zn/TiO2 catalysts for selective hydrogenation of butadiene. *Journal of Catalysis*, (2017). *347*, 185–196.

[42] Lee, H. Y., & Kale, G. M. Hydrothermal Synthesis and Characterization of Nano-TiO2. *International Journal of Applied Ceramic Technology*, (2008). *5*(6), 657–665.

[43] Rodriguez Quiroz, N., Padmanathan, A. M. D., Mushrif, S. H., & Vlachos, D. G. Understanding Acidity of Molten Salt Hydrate Media for Cellulose Hydrolysis by Combining Kinetic Studies, Electrolyte Solution Modeling, Molecular Dynamics Simulations, and 13C NMR Experiments. *ACS Catalysis*, (2019). *9*(11), 10551–10561.

[44] Chemie, S. Structure and Properties of Molten Salt Hydrates. *Electrochimica Acta* 1988 33(9), 1243–1250.

[45] Sen, S., Martin, J. D., & Argyropoulos, D. S. Review of cellulose non-derivatizing solvent interactions with emphasis on activity in inorganic molten salt hydrates. *ACS Sustainable Chemistry and Engineering*, (2013). *1*(8), 858–870.

[46] Minevich, A., Marcus, Y., & Ben-Dor, L. Densities of solid and molten salt hydrates and their mixtures and viscosities of the molten salts. *Journal of Chemical and Engineering Data*, (2004). *49*(5), 1451–1455.

[47] Ni, M., Leung, M. K. H., Leung, D. Y. C., & Sumathy, K. A review and recent developments in photocatalytic water-splitting using TiO2 for hydrogen production. *Renewable and Sustainable Energy Reviews*, (2007). *11*(3), 401–425.

[48] Panagiotopoulou, P., Christodoulakis, A., Kondarides, D. I., & Boghosian, S. Particle size effects on the reducibility of titanium dioxide and its relation to the water-gas shift activity of Pt/TiO2 catalysts. *Journal of Catalysis*, (2006). *240*(2), 114–125.

[49] G Grabowski, R., Grzybowska, B., Samson, K., Słoczyński, J., Stoch, J., & Wcisło, K. Effect of alkaline promoters on catalytic activity of V2O5/TiO2 and MoO3/TiO2 catalysts in oxidative dehydrogenation of propane and in isopropanol decomposition. *Applied Catalysis A, General*, (1995). *125*(1), 129–144.

[50] 2012. *Characterization Of Solid Materials And Heterogeneous Catalysts*. Weinheim: WILEY-VCH.

[51] Imelik, B. and Vedrine, J., n.d. *Catalyst Characterization.*

[52] [EB/OL].https://www.nanoscience.com/techniques/scanning-electron-microscopy/.

[53] Balachandran, U., & Eror, N. G. Raman spectra of titanium dioxide. *Journal of Solid State Chemistry*, (1982). *42*(3), 276–282.

[54] G. A. Tompsett, G. A. Bowmaker, R. P. Cooney, J. B. Metson, K. A. Rodgers and J. M. Seakins. The Raman Spectrum of Brookite, TiO2 (Pbca, Z = 8). *Journal of Raman Spectroscopy*. 1995(26), 57–62.

[55] Tran, T. Q., Zheng, W., & Tsilomelekis, G. Molten Salt Hydrates in the Synthesis of TiO2 Flakes. *ACS Omega*, (2019). *4*(25), 21302–21310.

[56] Bhagyaraj, S., n.d. *Synthesis Of Inorganic Nanomaterials*.

[57] Kumar, V. V., Naresh, G., Sudhakar, M., Tardio, J., Bhargava, S. K., & Venugopal, A. Role of Brønsted and Lewis acid sites on Ni/TiO2 catalyst for vapour phase hydrogenation of levulinic acid: Kinetic and mechanistic study. *Applied Catalysis A: General*, (2015). *505*, 217–223.

[58] Aramendí, M. A., Borau, V., Jiménez, C., Marinas, J. M., Porras, A., & Urbano, F. J. Determination of acid sites in solid catalysts by mass spectrometry. *Rapid Communications in Mass Spectrometry*, (1994). *8*(8), 599–602.

[59] Chareonlimkun, A., Champreda, V., Shotipruk, A., & Laosiripojana, N. Catalytic conversion of sugarcane bagasse, rice husk and corncob in the presence of TiO2, ZrO2 and mixed-oxide TiO2-ZrO2 under hot compressed water (HCW) condition. *Bioresource Technology*, (2010). *101*(11), 4179–4186.

[60] Kulkarni, A. P., & Muggli, D. S. The effect of water on the acidity of TiO2 and sulfated titania. *Applied Catalysis A: General*, (2006). *302*(2), 274–282.

[61] Manríquez, M. E., López, T., Gómez, R., & Navarrete, J. Preparation of TiO2-ZrO2 mixed oxides with controlled acid-basic properties. *Journal of Molecular Catalysis A: Chemical*, (2004). *220*(2), 229–237.

[62] Zhang, Y., Weidenkaff, A., & Reller, A. Mesoporous structure and phase transition of nanocrystalline TiO2. *Materials Letters*, (2002). *54*(5–6), 375–381.

[63] George W. Scherer.Sol-Gel Science: The Physics and Chemistry of Sol-Gel Processing. Harcourt Brace Jovanoarch: Boston,1990:21.